

The IceCube Neutrino Observatory

Contributions to ICRC 2017 Part V: Solar flares, Supernovae, Event reconstruction, Education & Outreach

Contents

1 Search for GeV neutrinos associated with solar flares with IceCube	
PoS (ICRC2017) 1010	6
2 Estimating the Sensitivity of IceCube to Signatures of Axion Production in a Galactic Supernova — PoS (ICRC2017) 892	14
3 Searching for Arbitrary Low-Energy Neutrino Transients with IceCube	
PoS (ICRC2017) 936	22
4 Deep Learning in Physics exemplified by the Reconstruction of Muon-Neutrino Events in IceCube — PoS (ICRC2017) 1057	30
5 Connecting Beyond the Research Community: IceCube Education, Outreach, and Communication Efforts — PoS (ICRC2017) 1072	38

35th International Cosmic Ray Conference — ICRC2017
10–20 July, 2017
Bexco, Busan, Korea

IceCube Collaboration Member List

M. G. Aartsen², M. Ackermann⁵², J. Adams¹⁶, J. A. Aguilar¹², M. Ahlers²⁰, M. Ahrens⁴⁴, I. Al Samarai²⁵, D. Altmann²⁴, K. Andeen³³, T. Anderson⁴⁹, I. Ansseau¹², G. Anton²⁴, C. Argüelles¹⁴, J. Auffenberg¹, S. Axani¹⁴, H. Bagherpour¹⁶, X. Bai⁴¹, J. P. Barron²³, S. W. Barwick²⁷, V. Baum³², R. Bay⁸, J. J. Beatty^{18,19}, J. Becker Tjus¹¹, K.-H. Becker⁵¹, S. BenZvi⁴³, D. Berley¹⁷, E. Bernardini⁵², D. Z. Besson²⁸, G. Binder^{9,8}, D. Bindig⁵¹, E. Blaufuss¹⁷, S. Blot⁵², C. Boehm⁴⁴, M. Börner²¹, F. Bos¹¹, D. Bose⁴⁶, S. Böser³², O. Botner⁵⁰, J. Bourbeau³¹, F. Bradascio⁵², J. Braun³¹, L. Brayeur¹³, M. Brenzke¹, H.-P. Bretz⁵², S. Bron²⁵, J. Brostean-Kaiser⁵², A. Burgman⁵⁰, T. Carver²⁵, J. Casey³¹, M. Casier¹³, E. Cheung¹⁷, D. Chirkin³¹, A. Christov²⁵, K. Clark²⁹, L. Classen³⁶, S. Coenders³⁵, G. H. Collin¹⁴, J. M. Conrad¹⁴, D. F. Cowen^{49,48}, R. Cross⁴³, M. Day³¹, J. P. A. M. de André²², C. De Clercq¹³, J. J. DeLaunay⁴⁹, H. Dembinski³⁷, S. De Ridder²⁶, P. Desiati³¹, K. D. de Vries¹³, G. de Wasseige¹³, M. de With¹⁰, T. DeYoung²², J. C. Díaz-Vélez³¹, V. di Lorenzo³², H. Dujmovic⁴⁶, J. P. Dumm⁴⁴, M. Dunkman⁴⁹, B. Eberhardt³², T. Ehrhardt³², B. Eichmann¹¹, P. Eller⁴⁹, P. A. Evenson³⁷, S. Fahey³¹, A. R. Fazely⁷, J. Felde¹⁷, K. Filimonov⁸, C. Finley⁴⁴, S. Flis⁴⁴, A. Franckowiak⁵², E. Friedman¹⁷, T. Fuchs²¹, T. K. Gaisser³⁷, J. Gallagher³⁰, L. Gerhardt⁹, K. Ghorbani³¹, W. Giang²³, T. Glauch¹, T. Glüsenskamp²⁴, A. Goldschmidt⁹, J. G. Gonzalez³⁷, D. Grant²³, Z. Griffith³¹, C. Haack¹, A. Hallgren⁵⁰, F. Halzen³¹, K. Hanson³¹, D. Hebecker¹⁰, D. Heereman¹², K. Helbing⁵¹, R. Hellauer¹⁷, S. Hickford⁵¹, J. Hignight²², G. C. Hill², K. D. Hoffman¹⁷, R. Hoffmann⁵¹, B. Hokanson-Fasig³¹, K. Hoshina^{31,a}, F. Huang⁴⁹, M. Huber³⁵, K. Hultqvist⁴⁴, M. Hünnefeld²¹, S. In⁴⁶, A. Ishihara¹⁵, E. Jacobi⁵², G. S. Japaridze⁵, M. Jeong⁴⁶, K. Jero³¹, B. J. P. Jones⁴, P. Kalaczynski¹, W. Kang⁴⁶, A. Kappes³⁶, T. Karg⁵², A. Karle³¹, U. Katz²⁴, M. Kauer³¹, A. Keivani⁴⁹, J. L. Kelley³¹, A. Kheirandish³¹, J. Kim⁴⁶, M. Kim¹⁵, T. Kintscher⁵², J. Kiryluk⁴⁵, T. Kittler²⁴, S. R. Klein^{9,8}, G. Kohnen³⁴, R. Koirala³⁷, H. Kolanoski¹⁰, L. Köpke³², C. Kopper²³, S. Kopper⁴⁷, J. P. Koschinsky¹, D. J. Koskinen²⁰, M. Kowalski^{10,52}, K. Krings³⁵, M. Kroll¹¹, G. Krückl³², J. Kunnen¹³, S. Kunwar⁵², N. Kurahashi⁴⁰, T. Kuwabara¹⁵, A. Kyriacou², M. Labare²⁶, J. L. Lanfranchi⁴⁹, M. J. Larson²⁰, F. Lauber⁵¹, D. Lennarz²², M. Lesiak-Bzdak⁴⁵, M. Leuermann¹, Q. R. Liu³¹, L. Lu¹⁵, J. Lünemann¹³, W. Luszczak³¹, J. Madsen⁴², G. Maggi¹³, K. B. M. Mahn²², S. Mancina³¹, R. Maruyama³⁸, K. Mase¹⁵, R. Maunu¹⁷, F. McNally³¹, K. Meagher¹², M. Medici²⁰, M. Meier²¹, T. Menne²¹, G. Merino³¹, T. Meures¹², S. Miarecki^{9,8}, J. Micallef²², G. Momenté³², T. Montaruli²⁵, R. W. Moore²³, M. Moulai¹⁴, R. Nahnauer⁵², P. Nakarmi⁴⁷, U. Naumann⁵¹, G. Neer²², H. Niederhausen⁴⁵, S. C. Nowicki²³, D. R. Nygren⁹, A. Obertacke Pollmann⁵¹, A. Olivas¹⁷, A. O'Murchadha¹², T. Palczewski^{9,8}, H. Pandya³⁷, D. V. Pankova⁴⁹, P. Peiffer³², J. A. Pepper⁴⁷, C. Pérez de los Heros⁵⁰, D. Pieloth²¹, E. Pinat¹², M. Plum³³, P. B. Price⁸, G. T. Przybylski⁹, C. Raab¹², L. Rädcl¹, M. Rameez²⁰, K. Rawlins³, I. C. Rea³⁵, R. Reimann¹, B. Relethford⁴⁰, M. Relich¹⁵, E. Resconi³⁵, W. Rhode²¹, M. Richman⁴⁰, S. Robertson², M. Rongen¹, C. Rott⁴⁶, T. Ruhe²¹, D. Ryckbosch²⁶, D. Rysewyk²², T. Sälzer¹, S. E. Sanchez Herrera²³, A. Sandrock²¹, J. Sandroos³², S. Sarkar^{20,39}, S. Sarkar²³, K. Satalecka⁵², P. Schlunder²¹, T. Schmidt¹⁷, A. Schneider³¹, S. Schoenen¹, S. Schöneberg¹¹, L. Schumacher¹, D. Seckel³⁷, S. Seunarine⁴², J. Soedingrekso²¹, D. Soldin⁵¹, M. Song¹⁷, G. M. Spiczak⁴²,

C. Spiering⁵², J. Stachurska⁵², M. Stamatikos¹⁸, T. Stanev³⁷, A. Stasik⁵², J. Stettner¹, A. Steuer³², T. Stezelberger⁹, R. G. Stokstad⁹, A. Stöbl¹⁵, N. L. Strotjohann⁵², G. W. Sullivan¹⁷, M. Sutherland¹⁸, I. Taboada⁶, J. Tatar^{9,8}, F. Tenholt¹¹, S. Ter-Antonyan⁷, A. Terliuk⁵², G. Tešić⁴⁹, S. Tilav³⁷, P. A. Toale⁴⁷, M. N. Tobin³¹, S. Toscano¹³, D. Tosi³¹, M. Tselengidou²⁴, C. F. Tung⁶, A. Turcati³⁵, C. F. Turley⁴⁹, B. Ty³¹, E. Unger⁵⁰, M. Usner⁵², J. Vandenbroucke³¹, W. Van Driessche²⁶, N. van Eijndhoven¹³, S. Vanheule²⁶, J. van Santen⁵², M. Vehring¹, E. Vogel¹, M. Vraeghe²⁶, C. Walck⁴⁴, A. Wallace², M. Wallraff¹, F. D. Wandler²³, N. Wandkowsky³¹, A. Waza¹, C. Weaver²³, M. J. Weiss⁴⁹, C. Wendt³¹, J. Werthebach²¹, S. Westerhoff³¹, B. J. Whelan², S. Wickmann¹, K. Wiebe³², C. H. Wiebusch¹, L. Wille³¹, D. R. Williams⁴⁷, L. Wills⁴⁰, M. Wolf³¹, J. Wood³¹, T. R. Wood²³, E. Woolsey²³, K. Woschnagg⁸, D. L. Xu³¹, X. W. Xu⁷, Y. Xu⁴⁵, J. P. Yanez²³, G. Yodh²⁷, S. Yoshida¹⁵, T. Yuan³¹, M. Zoll⁴⁴

¹III. Physikalisches Institut, RWTH Aachen University, D-52056 Aachen, Germany

²Department of Physics, University of Adelaide, Adelaide, 5005, Australia

³Dept. of Physics and Astronomy, University of Alaska Anchorage, 3211 Providence Dr., Anchorage, AK 99508, USA

⁴Dept. of Physics, University of Texas at Arlington, 502 Yates St., Science Hall Rm 108, Box 19059, Arlington, TX 76019, USA

⁵CTSPS, Clark-Atlanta University, Atlanta, GA 30314, USA

⁶School of Physics and Center for Relativistic Astrophysics, Georgia Institute of Technology, Atlanta, GA 30332, USA

⁷Dept. of Physics, Southern University, Baton Rouge, LA 70813, USA

⁸Dept. of Physics, University of California, Berkeley, CA 94720, USA

⁹Lawrence Berkeley National Laboratory, Berkeley, CA 94720, USA

¹⁰Institut für Physik, Humboldt-Universität zu Berlin, D-12489 Berlin, Germany

¹¹Fakultät für Physik & Astronomie, Ruhr-Universität Bochum, D-44780 Bochum, Germany

¹²Université Libre de Bruxelles, Science Faculty CP230, B-1050 Brussels, Belgium

¹³Vrije Universiteit Brussel (VUB), Dienst ELEM, B-1050 Brussels, Belgium

¹⁴Dept. of Physics, Massachusetts Institute of Technology, Cambridge, MA 02139, USA

¹⁵Dept. of Physics and Institute for Global Prominent Research, Chiba University, Chiba 263-8522, Japan

¹⁶Dept. of Physics and Astronomy, University of Canterbury, Private Bag 4800, Christchurch, New Zealand

¹⁷Dept. of Physics, University of Maryland, College Park, MD 20742, USA

¹⁸Dept. of Physics and Center for Cosmology and Astro-Particle Physics, Ohio State University, Columbus, OH 43210, USA

¹⁹Dept. of Astronomy, Ohio State University, Columbus, OH 43210, USA

²⁰Niels Bohr Institute, University of Copenhagen, DK-2100 Copenhagen, Denmark

²¹Dept. of Physics, TU Dortmund University, D-44221 Dortmund, Germany

²²Dept. of Physics and Astronomy, Michigan State University, East Lansing, MI 48824, USA

²³Dept. of Physics, University of Alberta, Edmonton, Alberta, Canada T6G 2E1

²⁴Erlangen Centre for Astroparticle Physics, Friedrich-Alexander-Universität Erlangen-Nürnberg,

D-91058 Erlangen, Germany

²⁵Département de physique nucléaire et corpusculaire, Université de Genève, CH-1211 Genève, Switzerland

²⁶Dept. of Physics and Astronomy, University of Gent, B-9000 Gent, Belgium

²⁷Dept. of Physics and Astronomy, University of California, Irvine, CA 92697, USA

²⁸Dept. of Physics and Astronomy, University of Kansas, Lawrence, KS 66045, USA

²⁹SNOLAB, 1039 Regional Road 24, Creighton Mine 9, Lively, ON, Canada P3Y 1N2

³⁰Dept. of Astronomy, University of Wisconsin, Madison, WI 53706, USA

³¹Dept. of Physics and Wisconsin IceCube Particle Astrophysics Center, University of Wisconsin, Madison, WI 53706, USA

³²Institute of Physics, University of Mainz, Staudinger Weg 7, D-55099 Mainz, Germany

³³Department of Physics, Marquette University, Milwaukee, WI, 53201, USA

³⁴Université de Mons, 7000 Mons, Belgium

³⁵Physik-department, Technische Universität München, D-85748 Garching, Germany

³⁶Institut für Kernphysik, Westfälische Wilhelms-Universität Münster, D-48149 Münster, Germany

³⁷Bartol Research Institute and Dept. of Physics and Astronomy, University of Delaware, Newark, DE 19716, USA

³⁸Dept. of Physics, Yale University, New Haven, CT 06520, USA

³⁹Dept. of Physics, University of Oxford, 1 Keble Road, Oxford OX1 3NP, UK

⁴⁰Dept. of Physics, Drexel University, 3141 Chestnut Street, Philadelphia, PA 19104, USA

⁴¹Physics Department, South Dakota School of Mines and Technology, Rapid City, SD 57701, USA

⁴²Dept. of Physics, University of Wisconsin, River Falls, WI 54022, USA

⁴³Dept. of Physics and Astronomy, University of Rochester, Rochester, NY 14627, USA

⁴⁴Oskar Klein Centre and Dept. of Physics, Stockholm University, SE-10691 Stockholm, Sweden

⁴⁵Dept. of Physics and Astronomy, Stony Brook University, Stony Brook, NY 11794-3800, USA

⁴⁶Dept. of Physics, Sungkyunkwan University, Suwon 440-746, Korea

⁴⁷Dept. of Physics and Astronomy, University of Alabama, Tuscaloosa, AL 35487, USA

⁴⁸Dept. of Astronomy and Astrophysics, Pennsylvania State University, University Park, PA 16802, USA

⁴⁹Dept. of Physics, Pennsylvania State University, University Park, PA 16802, USA

⁵⁰Dept. of Physics and Astronomy, Uppsala University, Box 516, S-75120 Uppsala, Sweden

⁵¹Dept. of Physics, University of Wuppertal, D-42119 Wuppertal, Germany

⁵²DESY, D-15738 Zeuthen, Germany

^aEarthquake Research Institute, University of Tokyo, Bunkyo, Tokyo 113-0032, Japan

Acknowledgment: The authors gratefully acknowledge the support from the following agencies and institutions: USA - U.S. National Science Foundation-Office of Polar Programs, U.S. National Science Foundation-Physics Division, University of Wisconsin Alumni Research Foundation, the Center for High Throughput Computing (CHTC) at the University of Wisconsin - Madison, the Open Science Grid (OSG) grid infrastructure and the Extreme Science and Engineering Discovery Environment (XSEDE); U.S. Department of Energy, and National Energy Research Scientific Computing Center; Particle Astrophysics research computing center at the University of Maryland; Institute for Cyber-Enabled Research at Michigan State University; Astroparticle Physics Computational Facility at Marquette University; Belgium - Funds for Scientific Research (FRS-FNRS and FWO), FWO Odysseus and Big Science programs, Belgian Federal Science Policy Office (Belspo); Germany - Bundesministerium für Bildung und Forschung (BMBF), Deutsche Forschungsgemeinschaft (DFG), Helmholtz Alliance for Astroparticle Physics (HAP), Initiative and Networking Fund of the Helmholtz Association; Deutsches Elektronen Synchrotron (DESY); Cluster of Excellence (PRISMA ? EXC 1098); High Performance Computing Cluster of the IT-Center of the RWTH Aachen; Sweden - Swedish Research Council, Swedish Polar Research Secretariat, Swedish National Infrastructure for Computing (SNIC), and Knut and Alice Wallenberg Foundation; Canada - Natural Sciences and Engineering Research Council of Canada, Calcul Québec, Compute Ontario, WestGrid and Compute Canada; Denmark - Villum Fonden, Danish National Research Foundation (DNRF); New Zealand - Marsden Fund, New Zealand; Australian Research Council; Japan - Japan Society for Promotion of Science (JSPS) and Institute for Global Prominent Research (IGPR) of Chiba University; Korea - National Research Foundation of Korea (NRF); Switzerland - Swiss National Science Foundation (SNSF).

Search for GeV neutrinos associated with solar flares with IceCube

The IceCube Collaboration[†]

[†] http://icecube.wisc.edu/collaboration/authors/icrc17_icecube

E-mail: gdewasse@icecube.wisc.edu

Since the end of the eighties and in response to a reported increase in the total neutrino flux in the Homestake experiment in coincidence with solar flares, solar neutrino detectors have searched for solar flare signals. Hadronic acceleration in the magnetic structures of such flares leads to meson production in the solar atmosphere. These mesons subsequently decay, resulting in gamma-rays and neutrinos of O(MeV-GeV) energies. The study of such neutrinos, combined with existing gamma-ray observations, would provide a novel window to the underlying physics of the acceleration process. The IceCube Neutrino Observatory may be sensitive to solar flare neutrinos and therefore provides a possibility to measure the signal or establish more stringent upper limits on the solar flare neutrino flux. We present an original search dedicated to low energy neutrinos coming from transient events. Combining a time profile analysis and an optimized selection of solar flare events, this research represents a new approach allowing to strongly lower the energy threshold of IceCube, which is initially foreseen to detect TeV neutrinos.

Corresponding author: G. de Wasseige*

IIHE-VUB, Pleinlaan 2, 1050 Brussels, Belgium

*35th International Cosmic Ray Conference
10-20 July, 2017
Bexco, Busan, Korea*

*Speaker.

1. Introduction

In 1988, the Homestake experiment reported an increase in the total number of neutrino events, potentially correlated with energetic solar flares [1]. J.N. Bahcall predicted that if this increase were indeed due to solar flares, it would lead to large characteristic signals in neutrino detectors [2]. In response, experiments such as Kamiokande [3] and SNO [4] performed several studies. Using different solar flare samples and analyses, the experiments were not able to confirm the potential signal seen by Homestake.

Solar flares convert magnetic energy into plasma heating and kinetic energy of charged particles such as protons [5]. Injected downwards from the coronal acceleration region, protons can interact with the dense plasma in the lower solar atmosphere through the processes indicated in Eq. 1.1 where the energy thresholds are 280 MeV and 180 MeV for p-p and p- α respectively.

$$p + p \text{ or } p + \alpha \longrightarrow \begin{cases} \pi^+ + X; & \pi^+ \longrightarrow \mu^+ + \nu_\mu; \mu^+ \longrightarrow e^+ + \nu_e + \bar{\nu}_\mu \\ \pi^0 + X; & \pi^0 \longrightarrow 2\gamma \\ \pi^- + X; & \pi^- \longrightarrow \mu^- + \bar{\nu}_\mu; \mu^- \longrightarrow e^- + \bar{\nu}_e + \nu_\mu \end{cases} \quad (1.1)$$

Due to their hadronic origin, solar flare neutrinos are of great interest for investigating proton acceleration and the subsequent interactions in the chromosphere. As demonstrated in several studies (see e.g. [6, 7, 8]), this neutrino flux extends from MeV up to a few GeV. Neutrino facilities sensitive to this energy regime could open a new window on solar flare physics and provide new constraints on e.g. the proton spectral index, as it is shown in these proceedings. In the following, we will focus on the IceCube Neutrino Telescope and its sensitivity to the high energy part of the neutrino spectrum from solar flares. Section 2 introduces a new event selection lowering the threshold of IceCube down to the GeV level. Combined with a dedicated time profile analysis described in Section 4, this selection allows IceCube to be sensitive to astrophysical transient events such as solar flares. The potential physics reach when applying this combination is described at the end of Section 4.

2. The IceCube Neutrino Observatory: from TeV to GeV

The IceCube Neutrino Observatory is a cubic-kilometer neutrino detector installed in the ice at the geographic South Pole between depths of 1450 m and 2450 m, completed in 2010 [9, 10]. A lower energy infill, the DeepCore subarray, includes 8 densely instrumented strings with smaller spacing between its optical modules (7 m versus 17 m in the IceCube strings) and its strings (72 m in average versus 125 m in IceCube) [11]. When a neutrino interacts in the neighborhood of the detector, the subsequent electromagnetic and/or hadronic cascade emit Cherenkov photons that can be detected by one or several of the 5160 optical modules distributed over the 1 km³ volume.

Originally dedicated to observe TeV neutrinos, IceCube has demonstrated the ability to extend its sensitivity to a larger energy range by the use of DeepCore. Indeed, since the observation of the first astrophysical neutrinos in 2013 [12], the IceCube collaboration has set several noteworthy limits on, among others, the existence of sterile neutrinos [13] and the spin-dependent WIMP-nucleon cross section [15] as well as competitive measurements of neutrino oscillation parameters [14]. The

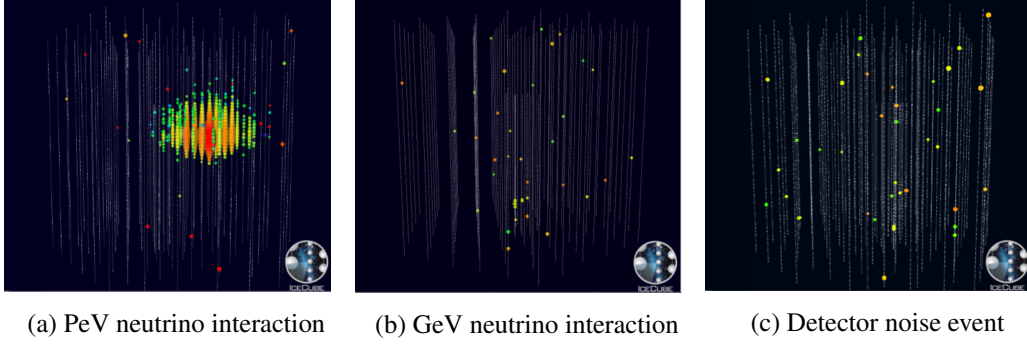


Figure 1: Examples of neutrino interactions as seen in IceCube. A typical GeV neutrino interaction is illustrated in [1b](#) while [1a](#) and [1c](#), respectively, show the well-known "Ernie" event in the PeV range and a detector-noise event (see the text for more details).

collaboration has also joined the worldwide multimessenger effort studying the highest energetic events in our Universe [[16](#), [17](#), [18](#)].

The work presented in these proceedings will demonstrate a new selection capable of extending the sensitivity to neutrino energies around 1 GeV as well as the use of external facilities/experiments to define a time window of interest. With these two tools, IceCube will be able to study astrophysical transient events down to GeV scales.

3. Selection of GeV events

The event selection presented here is optimized for neutrino interactions happening in the DeepCore volume. A softer trigger condition is implemented in this subdetector in order to increase the sensitivity to lower neutrino energies. Three hit optical modules satisfying a Hard Local Coincidence (HLC)¹ within a $2.5 \mu\text{s}$ time window are required to define an "event". Furthermore, the sample only contains events that *did not* fulfill the conditions to pass the running filters [[10](#)], except for the DeepCore Filter and either of two additional filters dedicated to low-energy neutrinos: the *Low-up* filter (LowUp) and/or the *Full-Sky-Starting* filter (FSS). The LowUp filter has been designed to target low-energy neutrinos coming from the Northern sky while the FSS filter uses parts of the detector as veto for incoming muon events, allowing to search for low-energy neutrinos from all directions. This results in a significant reduction of the number of atmospheric muons – from the original rate of 1400 Hz to 15 Hz – while retaining more than 98% of signal events.

As illustrated in [Fig.1](#), the main difference between TeV and GeV neutrino interactions is the amount of light emitted in the ice. Putting strong constraints on the number of optical modules hit eliminates neutrinos and remaining muons with an energy exceeding 5 GeV. A distinction is made between IceCube strings (i.e. strings with a spacing of 125 m) and DeepCore strings (i.e. with a 72 m average spacing) to optimize the selection of DeepCore events. An upper limit on the number of causally connected optical modules, i.e. the DOMs that have likely observed the same physics interaction, further helps to select low energy events. A GeV neutrino interaction produces a small cascade or a short track emitting light close to the interaction vertex, resulting in a small number

¹ At least two hit DOMs in a next- or next-to near neighbor vertical span in a time window of $\pm 1 \mu\text{s}$.

Table 1: Summary of the conditions required for an event to be selected as a GeV-like neutrino interaction.

Variable	Passing condition
Trigger $N_{\text{HLC-DOMS}}$	≥ 3
Passing filters	<i>DeepCore</i> or <i>DeepCore</i> + (<i>LowUp</i> and/or <i>FSS</i>)
$N_{\text{HLC-DOMS}}$ in IceCube strings	≤ 6
$N_{\text{HLC-DOMS}}$ in DeepCore strings	≤ 7
N_{DOMS} causally connected	≤ 10

of causally connected DOMs. A summary of the conditions required for an event to be selected as a GeV-like neutrino interaction is listed in Table 1.

3.1 Minimizing the contribution of pure noise events

Besides high energy muons and neutrinos that could still contaminate the low energy event sample, pure detector noise events may trigger DeepCore and pass the above selection. A detailed simulation of noise in the detector helps to estimate the potential contamination of accidental triggers caused by detector noise, hereafter referred to as "noise events". These include uncorrelated thermal noise, uncorrelated radioactive noise, and correlated scintillation noise [19]. About 6 Hz of pure noise survives the selection described above, being the dominant contribution of the event sample. It is therefore important to minimize this contribution.

Events which have hits that are causally connected are kept, while events containing many non-causally connected hits are removed. The causality between two hits is stated if their effective speed - i.e. the distance between the two hits divided by the time separation between them - is consistent with the speed of light in ice. Applying the causality condition significantly reduces the rate of detector noise events, from 15 Hz to 0.2 Hz.

3.2 Rate and detector stability

After the event selection described above, the data rate is around 0.2 Hz while more than 50% of the neutrino interactions below 5 GeV generated with *Genie* [20] with a generic E^{-2} spectrum pass the selection.

Even if this rate is still substantially larger than the expectation of atmospheric neutrinos, estimated to occur at the mHz level, the selection is sensitive both to single transient events as for an event-stacking analysis. The sensitivity depends on the stability of the detector once the event selection is applied. Fig. 2 shows the rate, smoothed with a low pass filter, for three periods of time occurring in 2011-2013. Even though Poissonian fluctuations are present, the overall behavior of the rate is constant along the seasons and the years.

The actual sensitivity of this event selection to astrophysical transient events depends on the characteristics of the event class itself. In the next section, we focus on solar flares, defining a specific framework that allows IceCube to be sensitive in the GeV energy range.

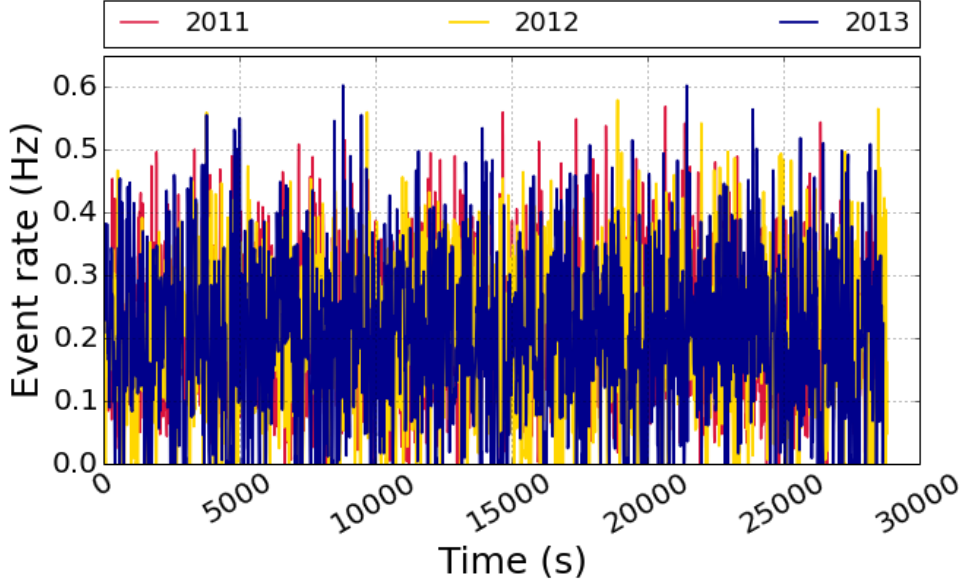


Figure 2: Detector rate using a 10 s smoothing and an order 3 low-pass butterworth filter. Three different periods of the year in 2011 (red), 2012 (yellow) and 2013 (blue) are shown. To prevent unblinding issues with future transient searches using the same event selection, the absolute time of the data has been omitted. Even though there are Poissonian fluctuations, the mean values, 0.22 Hz (2011), 0.20 Hz (2012) and 0.20 Hz (2013), are consistent with each other.

4. Solar flare application

The work presented in these proceedings uses the event selection described above to search for neutrinos from solar flares. As described in [21], one can select solar flares with high probability of pion production in order to optimize this search for neutrinos. Due to their common production channel through the decay of pions, gamma-rays and neutrinos are expected to be emitted simultaneously. Therefore, using observations from gamma-ray detectors such as Fermi-LAT [22] allows one to define solar flare events of interest as well as precise time windows for an optimal neutrino search.

It is also interesting to note that Fermi-LAT has been able to detect the impulsive phase in some of the latest solar flare events. These impulsive phases are characterized by a small full-width at half-maximum, narrowing down the neutrino search window to a few minutes. Moreover, the analysis of the gamma rays detected during these short phases reveals a relatively hard initial proton spectrum, with a spectral index around 3, as well as an enhanced gamma ray yield [23]. The long duration emissions, on the contrary, show a softer proton spectral index (between 4 and 6) and a spread of the gamma-ray emission over several hours. Focusing on the impulsive phase of bright events of the last solar cycle therefore increases the chance of a neutrino detection in coincidence with solar flares.

These proceedings focus on an observed event on March 7th, 2012, for which the Fermi-LAT instrument was able to detect both the impulsive and long duration emissions [23]. Furthermore, the Fermi collaboration could realize a spectral analysis of the impulsive phase. One can then

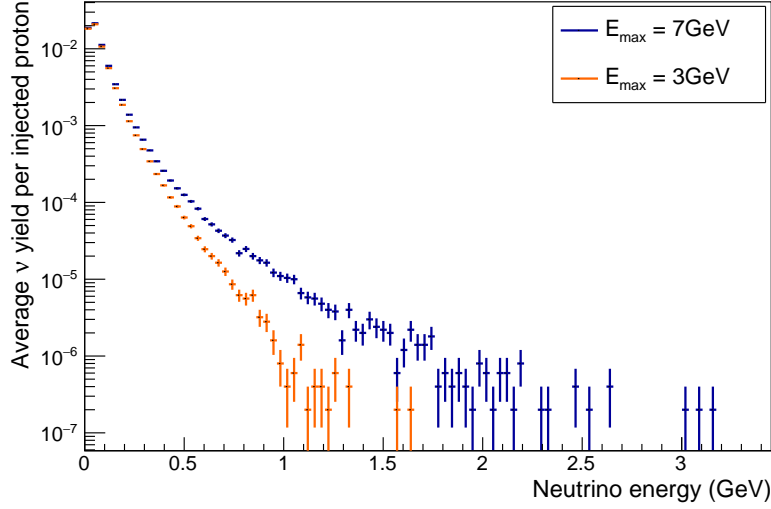


Figure 3: Average neutrino yield per injected proton with a spectral index of 3.2 and a upper cutoff of 7 GeV (blue) and 3 GeV (orange). A higher cutoff value leads to a higher neutrino yield in the energy range targeted by the event selection presented in this work.

define the optimal time window using gamma-rays with an energy greater than 500 MeV, focusing in this way on the energy range where the selection defined above is sensitive. In the following, the first 20 minutes of the March 7th, 2012 event as detected by Fermi-LAT will be considered.

Following the method described in [6, 24], using the proton spectral index extracted from gamma ray observations by Fermi-LAT [23] for this particular event, one can estimate the corresponding numbers of neutrino interactions detectable by IceCube. A potential upper cutoff of the proton spectrum has been discussed in several studies (see e.g. [25]). While an exponentially falling spectrum could be present after this cutoff, we use here a Heaviside step function in order to be conservative on the expected neutrino flux. The proton flux is therefore defined as $\frac{d\phi}{dE} = AE^{-\delta}H(E_{max} - E)$, where A is a normalisation constant, δ represents the spectral index and E_{max} is the upper cutoff. The effect of this upper cutoff on the subsequent neutrino flux is illustrated in Fig. 3, where the blue (orange) points show the average neutrino yield per injected proton with $\delta = 3.2$ and $E_{max} = 7$ GeV (3 GeV). A higher cutoff value leads to a higher neutrino yield in the energy range targeted by the event selection described in Section 3.

Table 2 shows the expected number of events passing the event selection described in Section 2 for different upper cutoff values. Fig. 4 illustrates these numbers together with the number of events required for a 1-, 3-, and 5-sigma deviation from the background expectation in a counting experiment. IceCube has the potential to find a signal or constrain this upper cutoff using the strength of the signal detected during this solar flare. The same procedure can and will be repeated for the brightest solar flare events from the 24th solar cycle listed in [26, 21].

5. Summary

These proceedings describe a new event selection that allows the IceCube telescope to be

Table 2: Expected number of solar flare neutrino events passing the selection described in Section 2 for different values of the upper cutoff. These numbers have been obtained assuming a proton spectral index of 3.2, averaged and derived from observations of the March 7th, 2012 event [23]. For comparison, the last line shows the background expectation.

Value of the upper cutoff	Expected number of events in IceCube
3 GeV	$19.5 \pm 0.3 + \text{Bkg}$
5 GeV	$43.2 \pm 0.4 + \text{Bkg}$
7 GeV	$94.3 \pm 0.7 + \text{Bkg}$
Bkg = No signal (2011)	264 ± 16

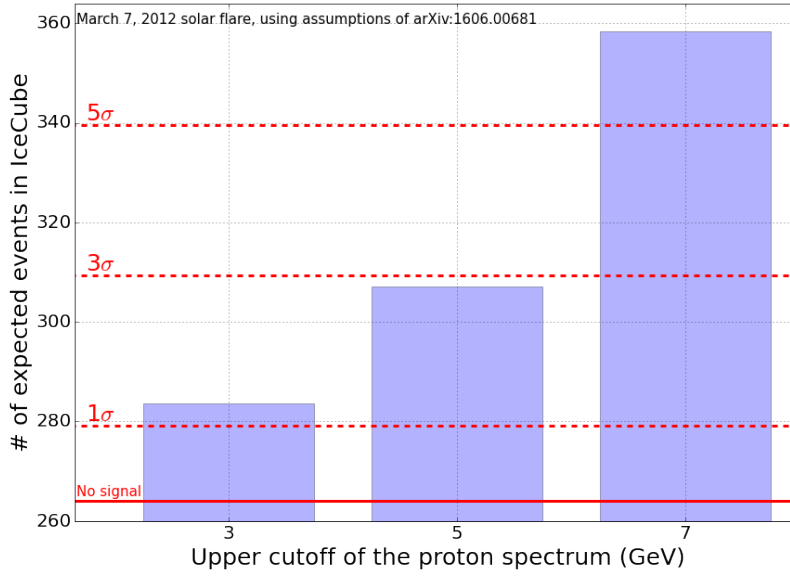


Figure 4: Comparison of the expected number of events in IceCube for the solar flare of March 7th, 2012 and the required number of events for a 1-, 3-, and 5-sigma deviation from background expectation in a counting experiment.

sensitive to GeV neutrinos, and therefore perform low-energy searches for astrophysical transient events, such as solar flares or gamma-ray bursts. This sensitivity to low energy neutrinos can be achieved by the use of electromagnetic observations to define the optimal time window for neutrino searches. An application to solar flare events, and especially to the bright event of March 7th, 2012, was presented. In the framework of solar flares, the Fermi-LAT instrument can define the events of interest as well as the optimal time window for a neutrino search. Assuming the proton spectral index derived from the Fermi-LAT observations, the number of events expected to pass the above selection has been established as a function of the upper cutoff of the proton spectrum. As illustrated in Fig. 4, IceCube has e.g. the potential to constrain this upper cutoff using the strength of the observed signal.

References

- [1] R. Davis, Nucl. Phys. B **48** (1996) 284.
- [2] J.N. Bahcall, Phys. Rev. Lett. **61** (1988) 2650.
- [3] K.S. Hirata *et al.*, Phys. Rev. Lett. **61** (1988) 2653.
- [4] B. Aharmim *et al.*, Astropart. Phys. **55** (2014) 1.
- [5] H.S. Hudson, Space Sci. Rev. **158** (2011) 5.
- [6] G. de Wasseige for the **IceCube** Collaboration, Moriond EW (2016). arXiv:1606.00681 [astro-ph.HE].
- [7] D. Fargion, JHEP **0406** (2004) 045.
- [8] G.E. Kocharov *et al.*, Il Nuevo Cimento 14C (1991) 4.
- [9] **IceCube** Collaboration, A. Achterberg *et al.*, Astropart. Phys. **26** (2006) 155.
- [10] **IceCube** Collaboration, M. G. Aartsen *et al.* JINST **12** (2017), P03012.
- [11] **IceCube** Collaboration, R. Abbasi *et al.*, Astropart. Phys. **35** (2012) 615.
- [12] **IceCube** Collaboration, M. G. Aartsen *et al.* Science **342** (2013) 1242856.
- [13] **IceCube** Collaboration, M. G. Aartsen *et al.*, Phys. Rev. Lett. **117** (2016), 071801.
- [14] **IceCube** Collaboration, M. G. Aartsen *et al.*, Nucl. Phys. B **908** (2016) 161.
- [15] **IceCube** Collaboration, M. G. Aartsen *et al.*, Eur. Phys. J. C **77** (2017), 146.
- [16] M. W. E. Smith *et al.*, Astropart. Phys. **45** (2013) 56.
- [17] **IceCube** Collaboration, M. G. Aartsen *et al.*, Astropart. Phys. **92** (2017) 30.
- [18] **IceCube** Collaboration, [PoS \(ICRC2017\) 1007](#) (these proceedings).
- [19] M. Larson, Ph.D thesis, University of Alabama, Tuscaloosa (2013).
- [20] C. Andreopoulos, Acta Phys. Polon. B **40** (2009) 2461.
- [21] G. de Wasseige *et al.*, (2015) arXiv:1505.05837 [astro-ph.HE].
- [22] W. B. Atwood *et al.*, Astrophys. J. **697** (2009) 1071.
- [23] M. Ajello *et al.*, Astrophys. Journ. **789** (2014) 20.
- [24] G. de Wasseige *et al.*, [PoS \(ICRC2015\) 1049](#) (2016).
- [25] Dj. Heristchi *et al.*, Sol.Phys. **49** (1976) 151.
- [26] M. Ackermann *et al.*, Astrophys. Journ. **787** (2014) 15.

Estimating the Sensitivity of IceCube to Signatures of Axion Production in a Galactic Supernova

The IceCube Collaboration[†]

[†] http://icecube.wisc.edu/collaboration/authors/icrc17_icecube

E-mail: sybenzvi@pas.rochester.edu, rcross@pas.rochester.edu,
tnguy51@u.rochester.edu

We describe the sensitivity of the IceCube Neutrino Observatory to the creation of axions in a Type II core-collapse supernova (SN II) in the Galaxy. Axions are a light dark matter candidate, and their existence is well-motivated as a solution to the strong CP problem. In a supernova, axions behave much like neutrinos, efficiently removing energy from the explosion and cooling the system. As a result, neutrino production in an SN II is suppressed in the presence of axions, mainly affecting the seconds-long tail of the SN II neutrino light curve. The IceCube Observatory is sensitive to large numbers of MeV neutrinos from an SN II, which produce a collective rise in the hit rates of all photomultipliers in the detector. We present a shape analysis that can be used with IceCube data to discriminate the axion production scenario from standard SN II models.

Corresponding authors: Segev BenZvi¹, Robert Cross^{*1}, Tri Nguyen¹

¹ *Department of Physics and Astronomy, University of Rochester, Rochester, NY, USA*

*35th International Cosmic Ray Conference – ICRC217 –
10-20 July, 2017
Bexco, Busan, Korea*

^{*}Speaker.

1. Introduction

Axions and axion-like particles (ALPs) are very light extensions to the Standard Model [1, 2, 3]. They were first hypothesized in 1977 as a consequence of the breaking of the Peccei-Quinn symmetry [4], which eliminates finely-tuned CP violating terms in the strong interaction. The Peccei-Quinn axion is a very light ($m_a \ll 1$ eV) pion-like pseudoscalar particle. It couples to Standard Model particles i with a strength g_{ai} proportional to its mass m_a . ALPs have properties similar to axions but m_a and g_{ai} can be independent.

Axions and ALPs may comprise a significant portion of the cold dark matter in the Universe, and a number of laboratory and astrophysical measurements are underway to study their properties. Most of these efforts focus on the coupling of axions and ALPs to photons. In the presence of an external magnetic field, ALPs can oscillate into photons and vice-versa [5]. In the laboratory, direct searches for axion-photon mixing are carried out using the LSW technique (“light shining through a wall”), in which sub-mm photons are transported through an opaque barrier by converting them to ALPs in a strong dipole magnet, and then converting them back to photons in a second magnet on the far side of the barrier. Indirect versions of the LSW measurement can be attempted by searching for photon-ALP oscillations in astrophysical sources with natural magnetic fields; for example, measurements of the conversion of axions from the Sun to keV photons [6], or measurements of anomalously hard TeV γ -ray spectra from distant AGN [7]. In the latter case the LSW “magnets” are the B fields of the AGN and Milky Way, and the “barrier” is the infrared extragalactic photon field which attenuates TeV γ rays from cosmologically distant sources. Indirect measurements of ALP-photon mixing are also possible in searches for oscillation-induced irregularities in the GeV and TeV spectra of gamma-ray sources [8, 9, 10].

Astrophysically, axions and ALPs are expected to behave like neutrinos, efficiently removing energy from stars and altering their evolution [11, 12, 13]. These effects carry over to high-luminosity astrophysical explosions such as Type II core-collapse supernovae (SNe II). With respect to standard astrophysical models, the production of axions in SNe II will create a significant excess of gamma rays [14, 15, 16] due to ALP-photon oscillations, as well as a significant deficit of neutrinos due to axion cooling (see e.g. [17] and [18]). The extreme luminosity of SNe II means that “gamma appearance” and “neutrino disappearance” measurements in a Galactic supernova can be used to achieve order-of-magnitude improvements in limits on the mass and coupling strength of axions and ALPs [16, 19]. Observations of a neutrino deficit are of particular interest because they are uniquely sensitive to the coupling of axions to nucleons [18, 20].

In this proceeding we describe the sensitivity of the IceCube Neutrino Observatory to the deficit of neutrinos in a Galactic SN II due to the effects of axion-nucleon coupling. We describe the IceCube detector and its sensitivity to supernovae in Section 2. The analysis technique and supernova model used are described in Section 3, followed by conclusions in Section 4.

2. Supernova Detection with IceCube

IceCube is a cubic kilometer Cherenkov detector located between 1.4 km and 2.4 km in the deep Antarctic ice below the South Pole. Using its array of 5160 digital optical modules (DOMs),

the detector is triggered by the Cherenkov light produced when neutrinos $\gtrsim 100$ GeV interact in or near the detector.

The typical energy of neutrinos from a core-collapse supernova is ~ 10 MeV, well below the trigger threshold of the main data acquisition system. The dominant interaction for supernova detection is $\bar{\nu}_e + p \rightarrow e^+ + n$. A 10 MeV e^+ , which is well above the Cherenkov threshold, loses its energy after traveling about 5 cm in the ice. Accounting for the Cherenkov emission of each positron, the efficiency of the DOMs, and the optical properties of the ice, a Galactic supernova will raise the count rate of each DOM by 2 Hz to 10 Hz for roughly 10 seconds, depending on the mass of the progenitor and its distance to Earth [21]. The average background count rate in the DOMs is about 280 Hz [21], and so the increase in the counts is not statistically significant at the level of individual channels. However, the correlated rise in the average background rate across the detector is highly statistically significant, with signal/background ratios $\gtrsim 10$ for an SN II located in the Milky Way [21].

In IceCube a dedicated supernova data acquisition system (SNDAQ) is used to search for neutrinos from a Galactic SN II in real time. SNDAQ monitors the background level in each DOM using a sliding 10-minute time window. In a central search window of width 0.5 s to 10 s, it maximizes the likelihood of a collective rate deviation $\Delta\mu$ across all DOMs,

$$\ln \mathcal{L}(\Delta\mu) = -\frac{1}{2} \left[\sum_{i=1}^{N_{\text{DOM}}} \left(\frac{r_i - (\langle r_i \rangle + \varepsilon_i \Delta\mu)}{\langle \sigma_i \rangle} \right)^2 + \ln \langle \sigma_i \rangle + \ln 2\pi \right], \quad (2.1)$$

where r_i is the hit rate of DOM i in the search window, $\langle r_i \rangle$ and $\langle \sigma_i \rangle$ are the mean and RMS uncertainty in the background rate of DOM i , and ε_i is the DOM efficiency. The maximum likelihood estimator $\Delta\hat{\mu}$ and its uncertainty $\sigma_{\Delta\hat{\mu}}$ are used to calculate the statistical significance $\xi = \Delta\hat{\mu} / \sigma_{\Delta\hat{\mu}}$. Statistically significant increases in $\Delta\mu$ produce real-time alerts for follow-up observations via the Supernova Early Warning System (SNEWS) [22].

3. Analysis

While SNDAQ produces alerts automatically and operates with $> 99\%$ uptime, the IceCube detector has not observed a Galactic supernova, and in fact no core-collapse supernovae have been observed in the Milky Way for hundreds of years. Therefore we perform an analysis of simulated data using the SN II neutrino light curve published by Fischer et al. [18], which compares an identical explosion with and without axion production in the proto-neutron star. In the following sections we describe the models and the shape analysis used to discriminate the two scenarios.

3.1 Supernova Reference and Axion Models

The process relevant for SNe II is nucleon-nucleon axion bremsstrahlung, described by the scattering $N_1 + N_2 \rightarrow N_3 + N_4 + a$. The phenomenological models used to describe axion-nucleon coupling are described in detail in [18], which assumes a Peccei-Quinn axion rather than an ALP. In brief, the coupling strength and axion mass scale like

$$g_{ai} = C_i \frac{m_N}{f_a} \approx 10^{-7} \left(\frac{m_a}{\text{eV}} \right) C_i, \quad m_a \approx 0.6 \text{ eV} \left(\frac{10^7 \text{ GeV}}{f_a} \right),$$

where f_a is the Peccei-Quinn energy scale, m_N is the nucleon mass, and $C_i \approx \mathcal{O}(0.1)$ is a constant that depends on the details of the hadronic axion model. Bounds on the axion-proton coupling from SN1987A yield

$$g_{ap} \lesssim 9 \times 10^{-10}, \quad m_a \lesssim 3 \times 10^{-2} \text{ eV}, \quad f_a \gtrsim 5 \times 10^8 \text{ GeV}$$

for the coupling strength and mass of the PQ axion [18].

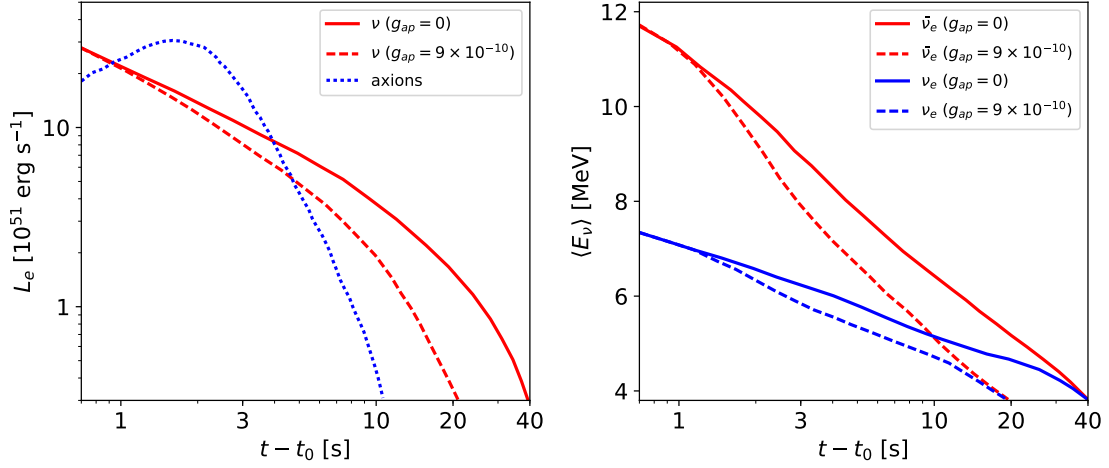


Figure 1: Neutrino and axion energy luminosity (left) and average neutrino energy for an SN II with an $18 M_\odot$ progenitor, as a function of time after core bounce t_0 (from [18]). At $t - t_0 = 10$ s, the nonzero axion-nucleon coupling reduces the neutrino luminosity by a factor of 2 and the average energy by 30% with respect to the reference model.

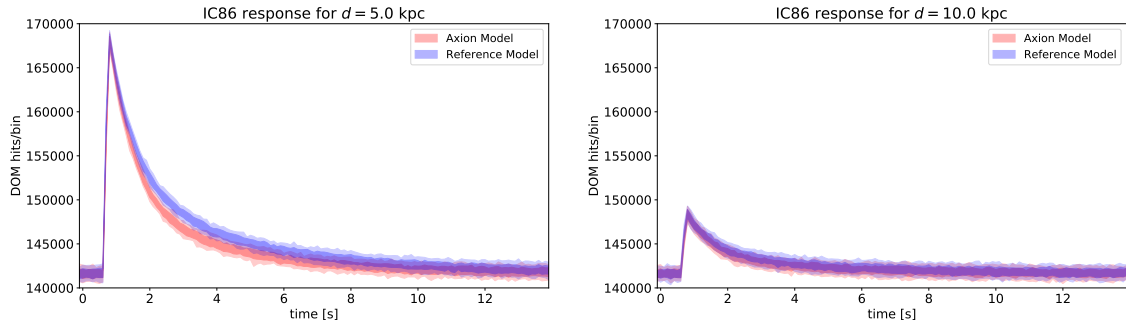


Figure 2: Simulated DOM hits in the completed 86-string configuration of IceCube (IC86) for a Galactic SN II located 5 kpc from Earth (left) and 10 kpc from Earth (right). A simulation using an $18 M_\odot$ progenitor from [18] was used to generate the DOM hits. The contours indicate the central 68% and 95% regions for 200 realizations of an explosion with axion production (“Axions”) and without (“Reference”).

Figure 1 shows the effect of axion production on the luminosity and average energy of neutrinos in an SN II from an $18 M_\odot$ progenitor [18]. An axion-proton coupling strength of $g_{ap} = 9 \times 10^{-10}$ has been assumed. While the neutrino luminosity at the breakout burst is not strongly affected by axion production, axions substantially reduce the length of the supernova cooling phase.

Ten seconds after the core bounce, the neutrino luminosity is reduced by a factor of two compared to the reference model without axion production.

Using the neutrino light curves and energy distributions shown in Figure 1, we have simulated the response of the full IceCube detector to an $18M_{\odot}$ SN II at a range of distances d from Earth. In Fig. 2 the summed DOM hits are plotted as a function of time after the explosion for $d = 5$ kpc and $d = 10$ kpc. The peak rate is unchanged if $g_{ap} \neq 0$, but the DOM hits in the cooling tail exhibit a clear decrease with respect to the reference model ($g_{ap} = 0$) before the rates return to the background level.

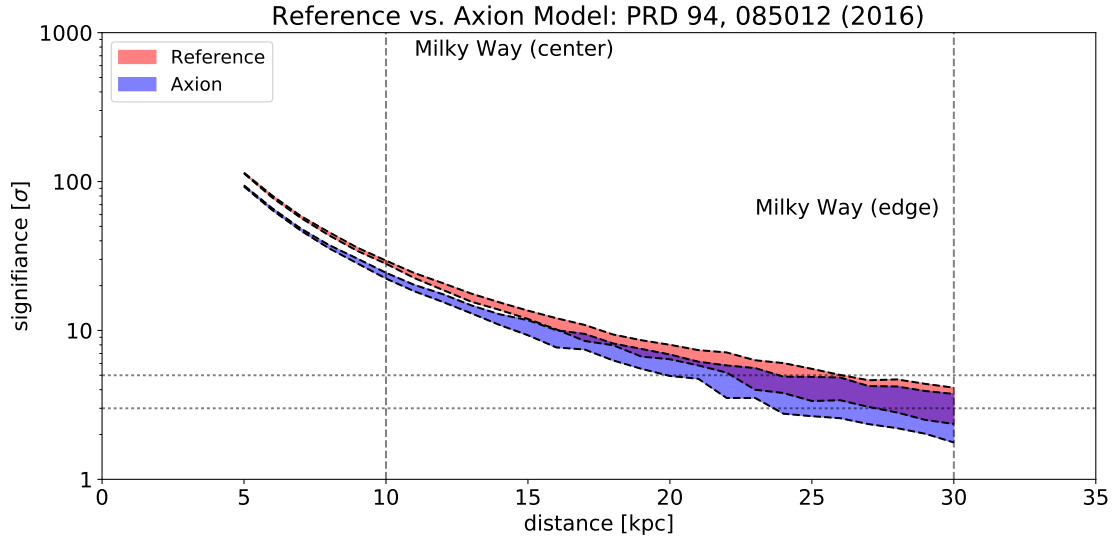


Figure 3: Sensitivity of IC86 to a Galactic SN II with an $18M_{\odot}$ progenitor as a function of distance to the source, using simulation results from [18]. The reference model refers to an explosion without axion production. The filled regions indicate the central 68% distribution of 200 realizations of each model. The dashed horizontal bands refer to the 3σ and 5σ thresholds.

Figure 3 shows the distribution of the detection significance ξ of Galactic SNe II as a function of distance from Earth, assuming the reference model $g_{ap} = 0$ and an axion production model $g_{ap} \neq 0$. In all cases a signal bin width of 10 s was used to compute the likelihood in eq. (2.1), and at each location 100 realizations of the SN II were generated to produce a 68% envelope for the significance distribution.

For any range of distances within 15 kpc of Earth the detection of this SN II is highly significant. The two scenarios are also relatively well-separated in that axion cooling strongly affects the strength of the signal for nearby explosions. For $d > 15$ kpc, the two scenarios become increasingly indistinguishable from each other and from fluctuations in the detector background.

3.2 Shape Analysis: Definition and Results

To discriminate between the reference and axion scenarios, we compute a test statistic based on the time required for 90% of the excess counts above background to be observed in IceCube. This quantity, which we denote t_{90} , is sensitive to relative differences in the shape of the cooling

tail shown in Fig. 2. Simulations indicate that t_{90} is insensitive to systematic uncertainties in the normalization of the neutrino emission model of up to 25%.

Given a realization of the $18M_{\odot}$ SN II at varying distances from Earth, we can construct a distribution of t_{90} for the scenario with no axion production (H_0) and the scenario with axion production (H_a). The resulting distributions are shown in Fig. 4 for two representative distances: 5 kpc from Earth (left) and 10 kpc from Earth (right). The distributions are normalized to provide an estimate of $p(t_{90}|H_i, d)$, the probability of observing a particular value of t_{90} given the distance d distance to the supernova and the model H_i under consideration.

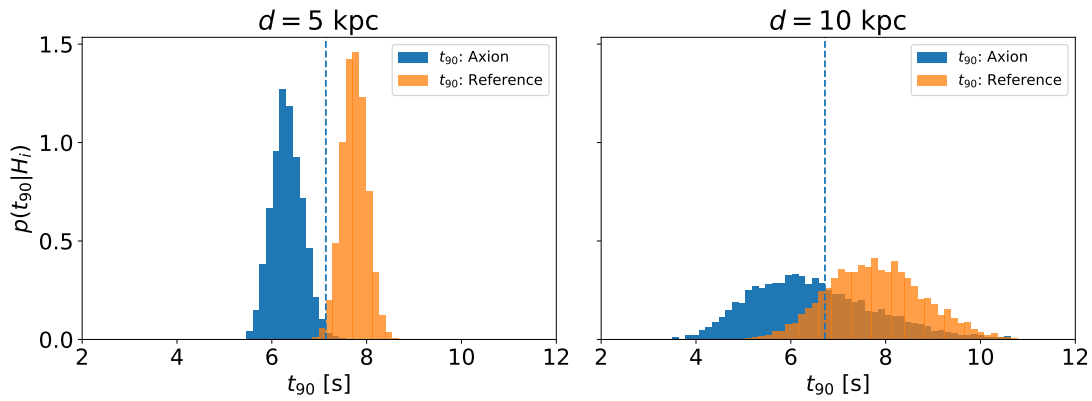


Figure 4: Distribution of t_{90} , the 90th percentile of the cumulative DOM hit light curve after baseline subtraction, for SN II models with axion production and without (“reference”), for an explosion 5 kpc and 10 kpc from Earth. The dashed line indicates an optimal cut on t_{90} that balances the false positive and false negative error obtained rates during model selection between the axion and reference models.

To discriminate between the two models, we construct a two-sided Neyman-Pearson hypothesis test that balances two quantities:

1. The Type I (or “false positive”) error rate α , defined as the tail probability of falsely rejecting the reference model H_0 . From Fig. 4,

$$\alpha = \int_{-\infty}^{t_{\text{cut}}} p(t_{90}|H_0) dt_{90}.$$

2. The Type II (or “false negative”) error rate, defined as the tail probability of falsely rejecting the axion model H_a . From Fig. 4,

$$\beta = \int_{t_{\text{cut}}}^{\infty} p(t_{90}|H_a) dt_{90}.$$

The value of t_{cut} used as the decision point between H_0 and H_a depends on the desired significance α and power $1 - \beta$ of the test. In Fig. 4 we indicate possible values of t_{cut} with a vertical dashed line. The particular choice shown in the figure balances the error rates α and β , but other choices are possible. For example, we may fix t_{cut} such that the test provides $\alpha \leq 0.0027$ (3σ) or $\alpha \leq 6 \times 10^{-7}$ (5σ) evidence against H_0 , and evaluate the resulting false negative rate β .

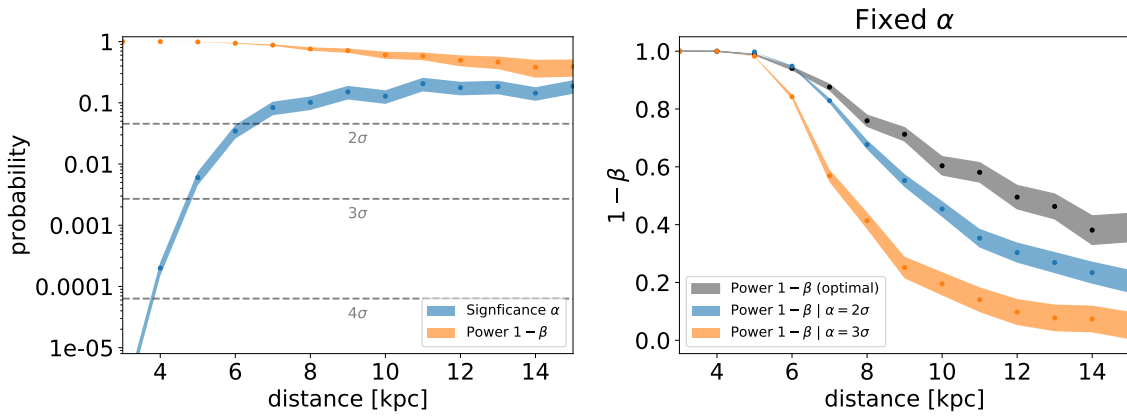


Figure 5: *Left:* dependence of the statistical significance α and statistical power $1 - \beta$ of an hypothesis test between the axion and reference models as a function of distance to the supernova, assuming a test boundary that balances the false positive and false negative error rates. The filled bands indicate the statistical uncertainties of the simulation. *Right:* dependence of the statistical power of the hypothesis test for fixed values of α . For reference, the top curve shows the statistical power for the “balanced” test boundary.

The statistical significance and power of the Neyman-Pearson test is shown in Figure 5 as a function of distance d to the supernova remnant. In the left panel of the figure, t_{cut} has been chosen to balance the false positive and false negative error rates α and β , as described in Fig. 4. In the right panel α has been fixed to the 2σ and 3σ thresholds, and the resulting values of t_{cut} and $1 - \beta$ were computed.

The constructed test suggests that IceCube would not be able to easily identify the axion production scenario in a supernova occurring 8 kpc away in the Galactic Center. In the case of the “balanced” test, simulations of an explosion at the Galactic Center produce $\alpha \approx 0.1$ and $1 - \beta \approx 0.8$. In the case where $\alpha = 0.0027$ (3σ), the typical threshold used for evidence against the reference hypothesis, the statistical power of the test is $\sim 40\%$; i.e., the production of axions is ruled out in the majority of realizations of the explosion.

However, the discrimination power of the test improves inversely with distance to the supernova. Simulations indicate that IceCube would exceed the 5σ discovery threshold for axion productions with supernovae located at $d \leq 3$ kpc from Earth.

4. Conclusions and Discussion

The simulation of a Galactic Type II supernova with and without the production of axions in the proto-neutron star suggests that IceCube has substantial sensitivity to the deficit of neutrinos caused by axion cooling within a limited detection horizon. The two-sided hypothesis test described in Section 3 is robust in the presence of systematic uncertainties in the model flux, and indicates that IceCube can reach the 5σ discovery threshold for SN II within 3 kpc of Earth. For an SN II in the Galactic Center, IceCube would provide 3σ evidence for axion production with moderate statistical power. Model discrimination becomes effectively impossible for distances beyond the Galactic Center.

Given the low rate of Type II supernovae in the Milky Way, a large degree of luck is required for IceCube to detect axion production in a Galactic SN II using the test described above. Therefore, the possibility of improving the significance of this detection, as well as extending the detection horizon, will be the subject of future work.

References

- [1] M. S. Turner, *Phys. Rept.* **197** (1990) 67–97.
- [2] K. A. Olive et al., *Chin. Phys.* **C38** (2014) 090001.
- [3] A. Ringwald, *Axions and Axion-Like Particles*, in *Proc. 49th Rencontres de Moriond*, pp. 223–230, 2014. [arXiv:1407.0546](#).
- [4] R. D. Peccei and H. R. Quinn, *Phys. Rev. Lett.* **38** (1977) 1440–1443.
- [5] G. Raffelt and L. Stodolsky, *Phys. Rev.* **D37** (1988) 1237.
- [6] E. Armengaud et al., *JINST* **9** (2014) T05002.
- [7] D. Horns, L. Maccione, M. Meyer, A. Mirizzi, D. Montanino, and M. Roncadelli, *Phys. Rev.* **D86** (2012) 075024.
- [8] D. Hooper and P. D. Serpico, *Phys. Rev. Lett.* **99** (2007) 231102.
- [9] **H.E.S.S.** Collaboration, A. Abramowski et al., *Phys. Rev.* **D88** (2013) 102003.
- [10] **Fermi-LAT** Collaboration, M. Ajello et al., *Phys. Rev. Lett.* **116** (2016) 161101.
- [11] G. G. Raffelt and D. S. P. Dearborn, *Phys. Rev.* **D36** (1987) 2211.
- [12] A. Friedland, M. Giannotti, and M. Wise, *Phys. Rev. Lett.* **110** (2013) 061101.
- [13] A. Ayala, I. Dominguez, M. Giannotti, A. Mirizzi, and O. Straniero, *Phys. Rev. Lett.* **113** (2014) 191302.
- [14] J. W. Brockway, E. D. Carlson, and G. G. Raffelt, *Phys. Lett.* **B383** (1996) 439–443.
- [15] A. Payez, C. Evoli, T. Fischer, M. Giannotti, A. Mirizzi, and A. Ringwald, *JCAP* **1502** (2015) 006.
- [16] M. Meyer, M. Giannotti, A. Mirizzi, J. Conrad, and M. Sánchez-Conde, *Phys. Rev. Lett.* **118** (2017) 011103.
- [17] M. S. Turner, *Phys. Rev. Lett.* **60** (1988) 1797.
- [18] T. Fischer, S. Chakraborty, M. Giannotti, A. Mirizzi, A. Payez, and A. Ringwald, *Phys. Rev.* **D94** (2016) 085012.
- [19] A. Payez, *A fresh look on the limit on ultralight axion-like particles from SN1987A*, in *Proc. AXION-WIMP 2014: Geneva, Switzerland*, pp. 121–124, 2014. [arXiv:1410.4404](#).
- [20] W. Keil, H.-T. Janka, D. N. Schramm, G. Sigl, M. S. Turner, and J. R. Ellis, *Phys. Rev.* **D56** (1997) 2419–2432.
- [21] **IceCube** Collaboration, R. Abbasi et al., *Astron. Astrophys.* **535** (2011) A109. [Erratum: *Astron. Astrophys.* 563, C1(2014)].
- [22] P. Antonioli et al., *New J. Phys.* **6** (2004) 114.

Searching for Arbitrary Low-Energy Neutrino Transients with IceCube

The IceCube Collaboration[†]

[†]http://icecube.wisc.edu/collaboration/authors/icrc17_icecube

E-mail: rcross@icecube.wisc.edu, segev.benzvi@icecube.wisc.edu

The IceCube Neutrino Observatory, located in the deep ice at the South Pole, is designed to observe neutrinos above 1 TeV; however, it is also highly sensitive to low-energy neutrinos from a Galactic Core Collapse Supernova (CCSN). SNDAQ, an online data acquisition and trigger system designed to observe CCSNe neutrino bursts in real time, is running with 99% uptime. In its current implementation, the time windows used by the SNDAQ trigger are tuned to typical supernova simulations and the observed signal from SN1987A. However, no galactic supernovae have been observed with high neutrino statistics so far, and many simulations do not produce an actual explosion. Therefore, it is wise to define a trigger that is not biased by simulations. To improve the sensitivity of the trigger to a much wider range of models, as well as unusual hadronic physics or physics beyond the Standard Model, we have implemented a time-domain search using the Bayesian Blocks algorithm. This technique allows the data themselves to determine the natural timescale of excess counts above background. The Bayesian Blocks window makes the SNDAQ trigger more robust to uncertainties in CCSN neutrino emission models. In addition, it also allows for general sub-threshold transient searches. We describe the implementation and performance of the Bayesian Blocks trigger and discuss improvements in the sensitivity of IceCube to supernovae in the Galaxy and its nearest satellites.

Corresponding authors: Robert Cross^{1,*} and Segev BenZvi¹

¹Department of Physics and Astronomy, University of Rochester, Rochester, NY, 14627, USA

*35th International Cosmic Ray Conference – ICRC217 –
10-20 July, 2017
Bexco, Busan, Korea*

*Speaker.

1. Core-Collapse Supernovae

Core-Collapse Supernovae (CCSNe) are among the most violent events in the Universe. CCSNe can be classified as any of Type Ib, Ic, or II, depending on the composition of the star. As the fuel within a massive star is synthesized into heavy nuclei, instabilities can occur which causes the star to violently collapse and then explode. A CCSN can put out 3×10^{53} erg in about 10 s [1], which is 250 times the energy the sun will emit over its entire lifetime. While Type Ia supernovae are caused by a runaway thermonuclear explosion and emit mostly electromagnetic radiation [2], all current models of CCSNe agree that roughly 99% of the gravitational energy of the collapsing star is released through neutrinos. On February 24, 1987, 24 neutrinos were detected around the world within a 13 second interval from SN1987A [3]. Hours later, the event was seen in the optical regime. Most of our current understanding of CCSNe is based upon the SN1987A neutrinos.

The detection of neutrinos from SN1987A prompted the development of CCSN theory, and the neutrinos from this event continue to be used to constrain models of core collapse. In addition, the scientific community has been building detectors waiting for the next supernova. It is estimated that only 3 galactic CCSNe happen every century [1], giving rise to thousands of neutrinos in a detector such as IceCube. With this information, we could measure the luminosity and time scales of the different stages of a core collapse and begin to differentiate between several CCSN models. In addition, we could combine pointing measurements from other detectors and localize the source. Finally, depending on the strengths and shapes of the signals we see, we could even probe the neutrino mass hierarchy [4].

The exact mechanisms behind CCSNe are currently unproven. The prevailing theory, based on 1D and 2D models, only tells us the broad sequence of events that occur during a CCSNe. The actual neutrino luminosity seen in a CCSN depends significantly on the mass of the progenitor star, the neutrino production model, and the distance to the source. Whatever method we use to detect a CCSN needs to handle a large range of unknowns.

2. Detection of Neutrinos with IceCube

The IceCube Neutrino Observatory [3] is a 1 km^3 water ice Cherenkov detector constructed at the geographic South Pole. The detector was constructed by drilling 2.5 km holes into the Antarctic ice sheet and lowering 86 cables (known as “strings”) instrumented with photosensors into the ice in a hexagonal grid layout. Each string is spaced about 125 m apart and each contains 60 Digital Optical Modules (DOMs) vertically separated by 17 m, for a total of 5160 DOMs. The DOMs are located between 1450 m to 2450 m below the surface of the ice. Each DOM contains a 10" hemispherical Hamamatsu R7081 photomultiplier tube and a complete autonomous data acquisition system.

IceCube is designed to detect TeV neutrino events; however, the neutrinos expected from CCSNe have energies of $\mathcal{O}(10 \text{ MeV})$. At these energies, the neutrinos will produce on average less than one photoelectron per DOM. However, with a sufficient number of low energy neutrinos interacting in the detector volume, a Galactic CCSN will produce a correlated rise in the dark rate of all of the DOMs.

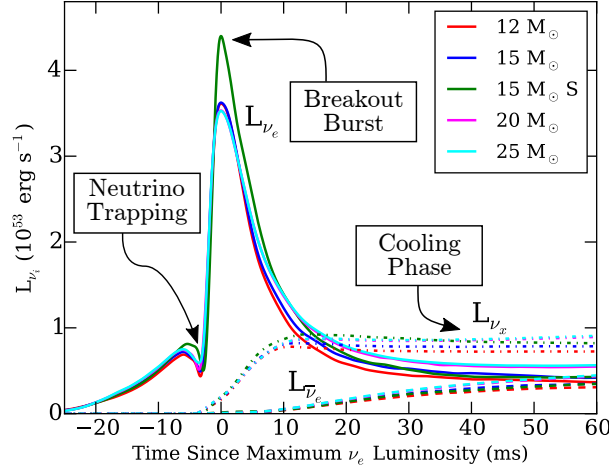


Figure 1: Neutrino luminosity of the breakout burst for five different simulated models before undergoing neutrino oscillations [4]. The solid lines show ν_e luminosity, the dashed lines show $\bar{\nu}_e$ luminosity, and the dot-dash lines show the luminosity of all other neutrino flavors. The point at which the core becomes dense enough to trap neutrinos can be seen as a small dip before the large spike in emissions at the breakout burst, after which neutrinos of all flavors are produced, and the overall luminosity decreases over the course of about 10 s as the remnant cools.

3. Supernova Trigger System

Because neutrinos from CCSNe are too low in energy to trigger the IceCube detector, we use the hit rates in the photomultipliers to search for supernova signals. The electronics in the DOMs count the number of times each DOM crosses a preset voltage threshold equivalent to 1/4 of a photoelectron. The DOMs are sampled at 40 MHz, and the threshold crossings are counted over 2^{16} clock cycles, which produces a hardware based fundamental time bin of 1.6384 ms. These rates are transmitted to the supernova data acquisition system (SNDQA) and are rebinned to 2 ms time bins for ease of further analysis [3].

The current implementation of the supernova trigger takes the 2 ms DOM hit rates and rebins the data further to various bin widths. The bin widths are optimized to detect signals that are consistent with current supernova models which predict neutrino emission on a variety of timescales. The time bases Δt are chosen to be 0.5 s, 1.5 s, 4.0 s and 10.0 s.

For each Δt , the hit rate for each DOM i , $r_i = N_i/\Delta t$, is calculated. Figure 2 shows the distribution of rates in a single DOM. The distribution of r_i has tails and can be described by the exponentially modified Gaussian distribution. For efficient calculation online, this is approximated as a Gaussian distribution.

The data are analyzed using a sliding window centered around the bin of interest. The structure of the sliding window is shown in Figure 3. To estimate the parameters of the Gaussian background, there is a moving interval of 300 s on either side of the bin of interest. From these 300 s regions, the expectation values of the rate and standard deviation $\langle r_i \rangle$ and $\langle \sigma_i \rangle$ are computed. There is also a 30 s exclusion zone between the background rate estimation windows and the bin of interest, so that very long-tailed signals do not influence the estimation of background rates.

The likelihood of a model which embodies a “collective rate deviation” that measures the

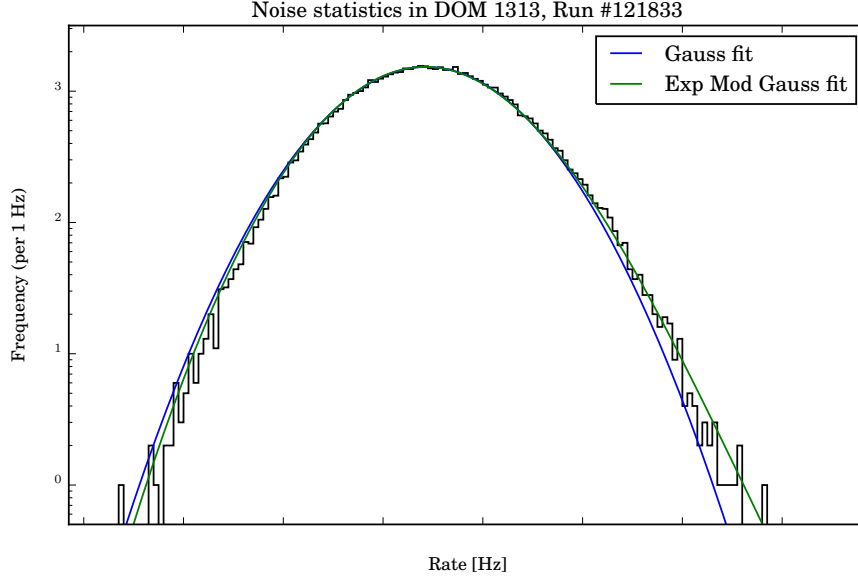


Figure 2: The distribution of the noise rate within a DOM. It is well described by the exponentially modified Gaussian distribution, but is approximated to a Gaussian to calculate likelihoods efficiently online.

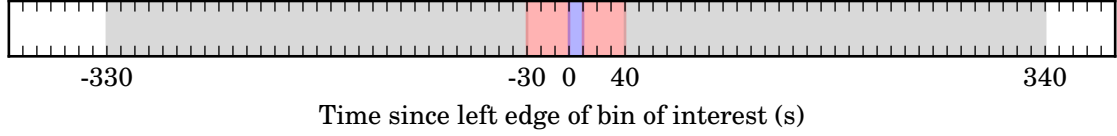


Figure 3: The structure of the sliding window in the current online analysis system. The blue zone in the center is the bin of interest. In this case, the time base Δt is 10 s. The red areas surrounding this bin represent the exclusion zone. These data are not used, so that heavy-tailed signals do not distort the background estimation. The grey areas show the data that are used to estimate the parameters for the distribution of background rates. The white areas show data outside the window. After the calculation, the window is shifted to the right by the timebase Δt .

isotropic rate deviation of all DOM noise rates r_i from their expectation values $\langle r_i \rangle$ with a DOM-dependent correction factor ε_i is

$$\mathcal{L}(\Delta\mu) = \prod_{i=1}^{N_{\text{DOM}}} \frac{1}{\sqrt{2\pi} \langle \sigma_i \rangle} \exp \left(-\frac{[r_i - (\langle r_i \rangle + \varepsilon_i \Delta\mu)]^2}{2 \langle \sigma_i \rangle^2} \right). \quad (3.1)$$

The likelihood is maximized for the $\Delta\mu$ parameter, and the “significance” of the bin is calculated as

$$\xi = \frac{\Delta\mu}{\sigma_{\Delta\mu}}. \quad (3.2)$$

4. Dynamic Histogramming

In this section, we discuss alternative methods to compute an optimal histogram binning which avoids the need to choose fixed values of Δt . These methods avoid the overhead of a template-based autocorrelation and are effective non-parametric approaches to observing an excess in real time.

4.1 Methods

The act of binning data is inherently lossy since it removes information about individual data points and groups them together, making them indistinguishable. If the bin size for a histogram is chosen to be too small, the noise in the data can dominate, and the signal cannot be seen. If the bin size is chosen to be too large, then one may completely miss important features in the underlying signal.

There are many methods of determining the optimal bin width in a non-arbitrary way. Scott's rule assumes a data set with Gaussian uncertainties, and varies the bin width while minimizing the integrated mean square error [5]. The Freedman-Daiconis rule expands upon Scott's rule by relaxing the Gaussian assumption [6]. In 2006, Knuth introduced a method that maximizes the posterior probability when comparing the data to piecewise constant models with uniform bin sizes [7].

4.2 Bayesian Blocks

Bayesian Blocks (BBlocks) is a dynamic histogramming method by Scargle that extends Knuth's rule even further. Instead of assuming that the model will consist of uniform bin widths, BBlocks allows the bin width to vary. BBlocks allows as many or as few bins as are needed in order to maximize the likelihood [8, 9].

The advantages of this method are clear: nothing needs to be assumed about the signal width or shape, gaps in data are handled seamlessly, it can easily be extended to real-time triggering, and it is very fast and lightweight. No information is wasted in generating the optimal partition. This algorithm can be applied to the detection of any transient signal, which is commonly done in the context of astrophysics. As such, there is a Python implementation of the algorithm included in AstroPy [10].

4.2.1 The Algorithm

The BBlocks algorithm compares the likelihood of the data to fit any of the possible piecewise constant models, or *partitions*. A partition is composed of one or many *blocks*, separated by *change points*. A data point or measurement is called a *cell*. For simplicity, the first and last cells are considered change points.

The algorithm considers every possible partition of the data. There are 2^N ways that N cells can be rearranged into partitions. The optimal partition is found by maximizing the “fitness” of each partition. The fitness function of a block is the likelihood of the data fitting the block model. In order to find the optimal partition efficiently, the fitness function must be “block additive”. In other words, the fitness function for a block must only depend on the data inside the block, and the fitness of a two block model must be the sum of the fitnesses of the two blocks independently.

The algorithm works by adding one data cell at a time and storing the best values of the fitness at every step. By doing this, data cells can be easily added and the best partitions and fitness values are updated. Once all data cells have been processed, the change points for the optimal partition are simply read out from the internal state of the algorithm. Figure 4 shows the evolution of the optimal partition as data cells are added. The algorithm adds and removes change points as needed while progressing through the data set.

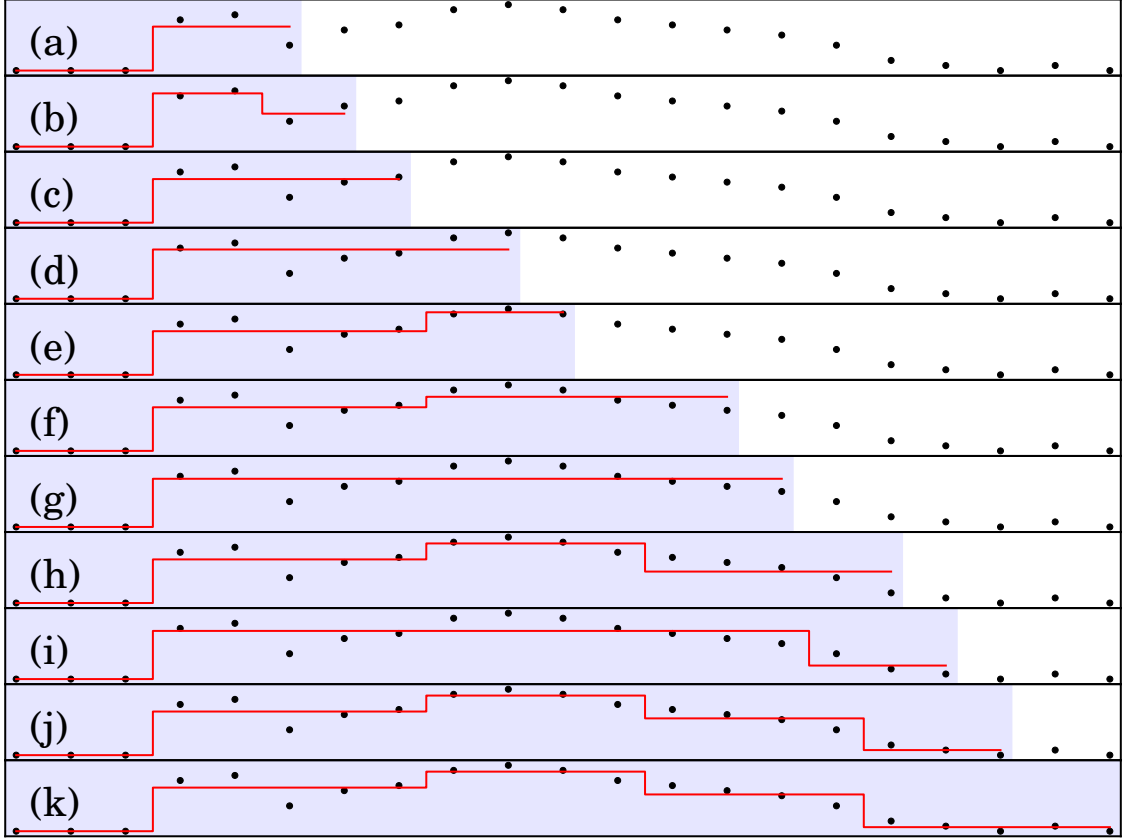


Figure 4: (a)-(k) shows the evolution of the best possible partition found by the Bayesian Blocks algorithm as data are added to the right hand side. Not all steps of the algorithm are shown. The dots show the data set used, generated by hand to showcase interesting behavior of the algorithm. The shaded area shows the data points included in the calculation at that step. The line shows the optimal partition found by the BBlocks algorithm using the included data points. At step (b), the algorithm finds that there is a secondary change point in the pulse, and at step (c), the change point is removed after another data point of information is added. You can see a similar thing happen as the algorithm goes from a 3-block model at step (i) to a 5-block model at step (j). The optimal piecewise constant model for the entire data set is found at the conclusion of the algorithm shown in (k).

By performing the search in this way, the algorithmic complexity of BBlocks is $\mathcal{O}(N^2)$. When you consider that there are 2^N choices of partitions, and that BBlocks gives an exact solution for finding the optimal partition, you can see how BBlocks can be used to detect a transient signal of any size or shape in a light curve [8, 9].

4.3 Block Fitness Function

A good choice of the block fitness function is the likelihood that the data fits the block model. For independent measurements that are approximately Gaussian, we can construct the likelihood of a given block ¹.

¹In the future, it would be interesting to implement an exponentially modified Gaussian fitness function into the BBlocks algorithm.

The likelihood of a measurement n is

$$\mathcal{L}_n = \frac{1}{\sigma_n \sqrt{2\pi}} e^{-\frac{1}{2} \left(\frac{x_n - \lambda}{\sigma_n} \right)^2}, \quad (4.1)$$

where λ is the model amplitude of the block being tested. The block likelihood is therefore

$$\mathcal{L}^{(k)} = \prod_n^{\text{in block } k} \mathcal{L}_n = \frac{(2\pi)^{-\frac{N_k}{2}}}{\prod_m \sigma_m} e^{-\frac{1}{2} \sum_n \left(\frac{x_n - \lambda}{\sigma_n} \right)^2}. \quad (4.2)$$

Maximizing the likelihood, taking the log, and removing model independent constants [8, 9], we get

$$\log \mathcal{L}_{\max}^{(k)} = \frac{b_k^2}{4a_k}, \quad (4.3)$$

where $a_k = \frac{1}{2} \sum_n \frac{1}{\sigma_n^2}$ and $b_k = -\sum_n \frac{x_n}{\sigma_n^2}$.

4.4 Prior on Number of Blocks and Type I Errors

The number of blocks N_{blocks} is a free parameter in this algorithm, so we must choose a prior probability distribution for the parameter. By default, a uniform distribution is selected as the prior distribution on the number of blocks. This is not very useful, as it causes the algorithm to return a partition with one block per data cell, since adding more blocks to match the data would always increase the likelihood. To solve this problem, we must adopt a penalty for adding more blocks.

Scargle chooses to use a single parameter geometric prior for efficient calculations. After normalization, for N data cells, the prior is

$$P(N_{\text{blocks}}) = \frac{1 - \gamma}{1 - \gamma^{N+1}} \gamma^{N_{\text{blocks}}}. \quad (4.4)$$

With this choice, the log difference (ignoring the normalization, as this will be a constant in all models) in the prior is simply given by

$$\ln \left[\frac{P(K+1)}{P(K)} \right] = \ln \gamma. \quad (4.5)$$

This choice of γ effectively tunes the sensitivity of BBlocks, which can be very useful in a trigger. The rate at which the BBlocks algorithm will falsely identify a background fluctuation as a real change point is denoted p_0 . By running the algorithm on large amounts of background-only simulated data, we can tune the “false positive” rate p_0 in terms of the parameter γ . Thus, BBlocks can be tuned to any desired false positive rate.

4.5 Applications to SNDAQ

Simulated data were generated from the DOM noise distributions with light curves from several CCSN models positioned at various distances from Earth. The data were analyzed using the BBlocks algorithm and the rate of true positive detections were recorded. Figure 5 shows the results of these trials.

By raising the false positive rate p_0 , we can effectively extend the detection “horizon” of IceCube to more distant sources. The cost is an increase in the rate of spurious detections, but this increase is tunable and predictable. Note that the sensitivity of the detector depends strongly on the CCSN model used.

5. Future Work

We have implemented a nonparametric algorithm which allows the data themselves to choose the optimal binning scheme based on statistically significant changes in the hit rate. This allows for a tunable error rate which can be used to increase sensitivity to distant objects, with the compromise of seeing more false positives.

Given that the Galactic CCSN rate is about one in every 30 years, it is also notable that our algorithm can be used to search for many kinds of astrophysical transients (such as Fast Radio Bursts) while we wait for the next supernova. This would be a considerable advantage over the existing real-time detection system.

We are currently implementing and deploying BBlocks in the live analysis system to provide real-time alerts. Additional technical changes are planned, such as using the exponentially modified Gaussian fitness function.

References

- [1] S. M. Adams, C. S. Kochanek, J. F. Beacom, M. R. Vagins, and K. Z. Stanek, *The Astrophysical Journal* **778** (2013) 164.
- [2] W. P. Wright, J. P. Kneller, S. T. Ohlmann, F. K. Roepke, K. Scholberg, and I. R. Seitenzahl, *Phys. Rev.* **D95** (2017) 043006.
- [3] R. Abbasi et al., *Astronomy & Astrophysics* **535** (Nov., 2011) A109.
- [4] J. Wallace, A. Burrows, and J. C. Dolence, *The Astrophysical Journal* **817** (2016) 182.
- [5] D. W. Scott, *Biometrika* **66** (1979) 605–610.
- [6] D. Freedman and P. Diaconis, *Probability theory and related fields* **57** (1981) 453–476.
- [7] K. H. Knuth, *arXiv: physics/0605197* (May, 2006).
- [8] J. D. Scargle, *The Astrophysical Journal* **504** (Sept., 1998) 405.
- [9] J. D. Scargle, J. P. Norris, B. Jackson, and J. Chiang, *The Astrophysical Journal* **764** (Feb., 2013) 167.
- [10] T. P. Robitaille et al., *Astronomy & Astrophysics* **558** (2013) 9.

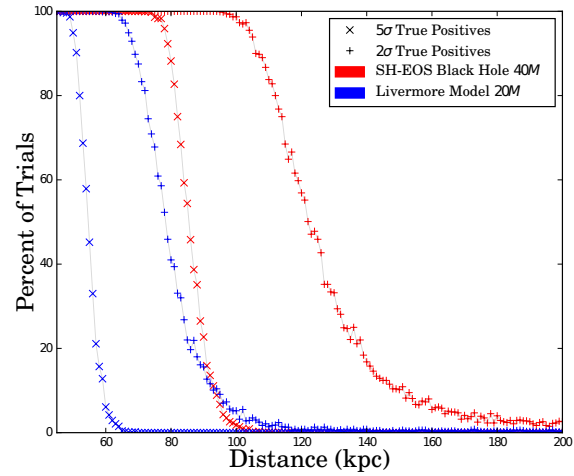


Figure 5: Plot showing the probability positively identifying a signal generated via simulated light curves at various distances. There are two curves for each model, each with the BBlocks algorithm tuned to two different values of p_0 corresponding to 5σ and 2σ significance that a detected edge is a false positive over a 500 s window. 1000 data sets were generated for each distance, and each data set was re-binned to 0.5 s.

Deep Learning in Physics exemplified by the Reconstruction of Muon-Neutrino Events in IceCube

The IceCube Collaboration[†]

[†] http://icecube.wisc.edu/collaboration/authors/icrc17_icecube

E-mail: mirco.huennefeld@tu-dortmund.de

Recent advances, especially in image recognition, have shown the capabilities of deep learning. Deep neural networks can be extremely powerful and their usage is computationally inexpensive once the networks are trained. While the main bottleneck for deep neural networks in the traditional domain of image classification is the lack of sufficient labeled data, this usually does not apply to physics where millions of Monte Carlo simulations exist.

The IceCube Neutrino Observatory is a Cherenkov detector deep in the Antarctic ice where the reconstruction of muon-neutrino events is one of the key challenges. Due to limited computational resources and the high data rate, only simplified reconstructions limited to a small subset of data can be run on-site at the South Pole. However, in order to perform online analysis and to issue real-time alerts, a fast and powerful reconstruction is necessary.

This paper demonstrates how deep learning techniques such as those used in image recognition can be applied to IceCube pulses in order to reconstruct muon-neutrino events. These methods can be generalized to other physics experiments.

Corresponding authors: Mirco Hünnefeld^{*1}

¹ *Dept. of Physics, TU Dortmund University, D-44221 Dortmund, Germany*

*35th International Cosmic Ray Conference
10-20 July, 2017
Bexco, Busan, Korea*

^{*}Speaker.

1. Introduction

The IceCube Neutrino Observatory is a neutrino detector located at the South Pole instrumenting a cubic kilometer of glacial ice. The detector consists of 5160 digital optical modules (DOMs) installed on 86 vertical strings at depths between 1450m and 2450m. These strings are deployed on an approximately triangular grid with a string-to-string spacing of about 125 m. [1]

In order to perform online analyses at the South Pole and to enable rapid follow-up observations, a realtime analysis framework for the IceCube neutrino observatory was implemented. The online processing and filtering system [1] calibrates the recorded DOM waveforms, extracts pulses from the waveforms and performs some basic event reconstructions. With the help of these reconstructions about 1 % of all triggered events are selected by dedicated online filters for further on-site processing (Online L2 Selection). One of the multiple online filters in place is the Level2 Online Muon Filter which aims to select well reconstructed track-like events of muons produced in charged current interactions of muon neutrinos. Given the hardware limitations at the South Pole, events from the Online L2 Selection must be processed within about 30s to prevent pileup. The limited computational resources and the high data rate pose a key challenge to obtaining an accurate event reconstruction. While more sophisticated reconstruction methods exist [2], their usage on-site becomes intractable when taking their runtime into account which can require minutes to hours for a single event. [3]

One possible solution to obtain powerful event reconstructions, while keeping the computational complexity low, is the use of deep learning techniques. Recent advances in image recognition [4] have shown the capabilities of deep convolutional networks. These networks belong to the class of representation-learning methods [5]. They are capable of processing raw data and of creating an abstract level of representation. Once the networks are trained, their usage is computationally inexpensive, while the reconstruction accuracy can be improved compared to conventional methods. The network performs a set amount of mathematical operations on the input data resulting in a very stable runtime that is essentially independent of the input. In comparison, runtimes of currently used on-site reconstructions are highly dependent on the input. These characteristics make deep learning methods an excellent candidate for powerful and fast on-site reconstructions.

2. Hexagonally shaped Data and Network Architecture

An IceCube muon-neutrino simulation dataset is used with a simulated neutrino spectrum of E^{-1} and an energy range from 100GeV to 10PeV. For the results shown in this paper, the neutrino spectrum is reweighed to an unbroken power-law flux with $E^{-2.13}$ according to [6]. Only track-like events are used, where the muon resulting from the charged-current neutrino interaction comes within 60m of the detector. Approximately 34,000 events are used for each of the test and validation set, while the training dataset consists of approximately 3 million events. The framework Tensorflow[7] is used in combination with the programming language Python¹. Training of the convolutional neural network is performed on an NVIDIA Tesla P40² and takes about a week.

¹<https://www.python.org/>

²<https://images.nvidia.com/content/pdf/tesla/184427-Tesla-P40-Datasheet-NV-Final-Letter-Web.pdf>

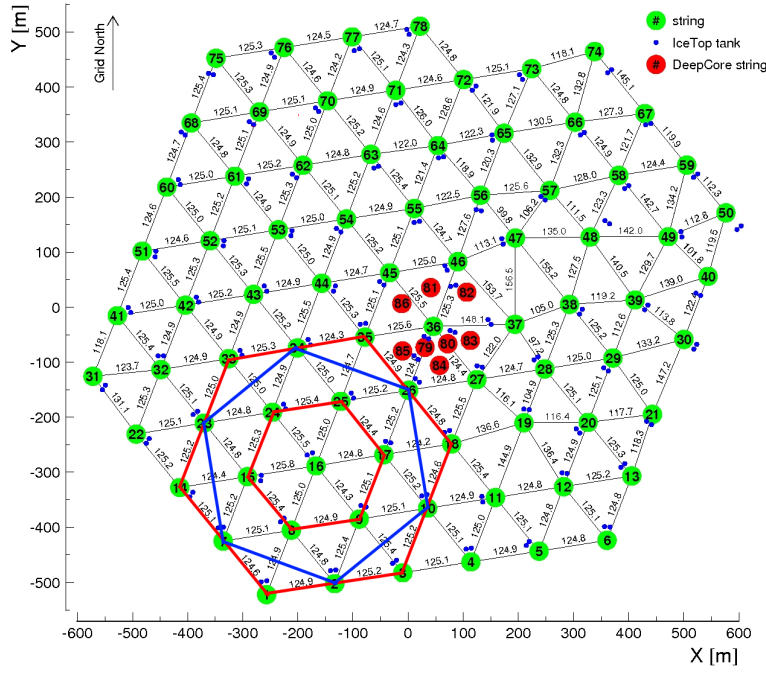


Figure 1: An on-top view of the IceCube detector is shown. The in green depicted 78 strings are on an approximately triangular grid, while the DeepCore strings painted in red are installed in a denser configuration. The hexagons around String 16 show the shape of hexagonal convolution kernels with 7, 13 and 19 included strings.

Figure 1 illustrates the geometry of the IceCube detector. The 86 strings of the IceCube detector, which each hold 60 DOMs, are divided into two detector parts. The first 78 strings are arranged in an hexagonal configuration. In the typical use cases of convolutional layers, the convolution is performed on orthogonal coordinate systems. The convolutional operators in Tensorflow therefore only support convolutions on such coordinate systems. In order to use the convolutional operators, the input data needs to be transformed. For this purpose, the hexagonally shaped data is transformed as described in Fig. 2. In a similar fashion, hexagonally shaped convolutional filters as shown in Fig. 1 are obtained and used for the convolutional layers.

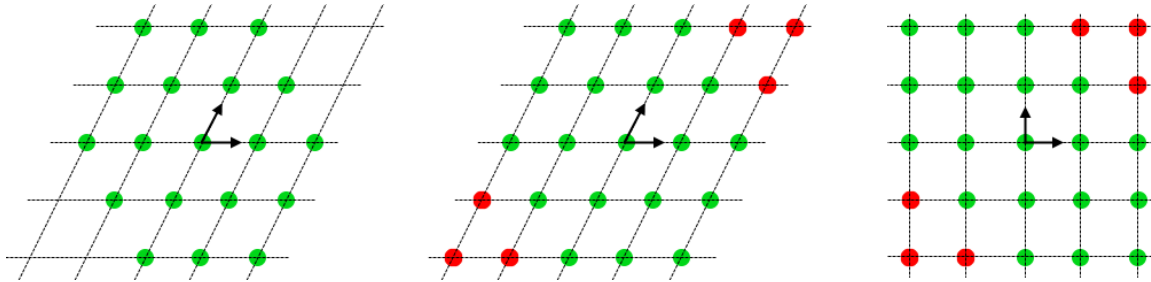


Figure 2: Hexagonally shaped data on the left (green dots) can be transformed into an orthogonal grid on the right by padding with zeros (red dots) and then shifting the rows, so that they align. Hexagonally shaped convolution filters are obtained with the same transformation.

The input data consists of one temporal and three spatial dimensions. For every DOM there is a series of pulses of arbitrary length. Each of these pulses consists of an arrival time and a charge. The pulse series of arbitrary length are condensed into 7 variables consisting of: sum of all charges, number of pulses, time of first pulse, time of last pulse, average time of pulses,

standard deviation of pulse times and highest pulse charge. The first 78 strings are mapped onto an orthogonal 10×10 grid via the described transformation. No transformation is applied to the DeepCore strings. Instead, the x- and y-dimensions of the DeepCore strings are reduced to a single dimension representing the string number. As a result, the input tensor has dimensions $(10 \times 10 \times 60 \times 7)$ and $(8 \times 60 \times 7)$ for the hexagonally arranged strings 1 through 78 and the 8 DeepCore strings, respectively. A different approach with a binning in time, where each bin holds the sum of all charges of the pulses within that time bin, achieves a similar accuracy as the results shown in section 3.

The input of the 78 hexagonally arranged strings is fed into six 3D convolutional layers with hexagonally shaped kernels (Fig. 1), while the DeepCore input is processed by four 2D convolutional layers. The 3D convolution is performed over the three spatial dimensions $(10 \times 10 \times 60)$. Similarly, the 2D convolution is applied on the two spatial dimensions (8×60) of the DeepCore input. The output of these convolutional layers is flattened, combined, and used as input to seven fully connected layers. The last fully connected layer has an output node for every target label. Currently, 14 different labels are being reconstructed such as the neutrino energy, the muon energy and the arrival direction of the muon.

In addition, the input data as well as the target labels are normalized to have a mean of 0 and a standard deviation of 1. Since the use of batch normalization [8] makes the training of arbitrary activation functions tractable, a combination of different activation functions is used. The motivation for this is that each activation function has a specific use case for which it is well suited. A combination of different activation functions might, therefore, be better suited to approximate complex problems. During training of the neural network, the learning rate of the gradient descent minimizer and the dropout rate are gradually decreased from 10^{-2} to 10^{-7} and from 0.2 to 0.05, respectively. Dropout[9] is a regularization technique, where a certain rate (dropout rate) of neurons are dropped during training. This prevents overfitting and makes the network more robust, as it cannot rely on the output of a single neuron. In connection with the high amount of training data and the comparably low complexity of the model, only a small amount of dropout is needed to prevent overfitting.

It should be noted that the architecture and settings for the neural network as described above are not yet fully optimized. Improvements through further optimization are expected.

3. Runtime and Performance

As mentioned in section 1, one of the key challenges for an on-site reconstruction is the runtime requirement. The Level2 Online Muon Filter, which includes several track and energy reconstructions, is one of the multiple filters being run on the Online L2 Selection. Its average runtime is about 273 ms/event. However, the runtime is highly dependent on the event, with a standard deviation of 605 ms/event. Single, very luminous events can require several seconds to process. In comparison, the neural network as described in section 2 has a runtime of about 20 ms/event on an NVIDIA Quadro M1000M and a runtime of approximately 2 ms/event on an NVIDIA Tesla P40. For the NVIDIA Tesla P40 the bottleneck appears not to be the prediction itself, but the time needed to feed the data into the network. A direct comparison between the runtimes, however, is difficult because the Level2 Online Muon Filter is performed on a CPU. In addition, the runtime

of the neural network is very stable with a standard deviation of less than 5 ms/event. The network always performs the same number of mathematical operations regardless of how luminous the event is. Therefore, the reconstruction by the neural network could be added to the Level2 Online Muon Filter without violating the runtime restrictions. Moreover, if more severe limitations were required, the network could easily be pruned with only little effects on the reconstruction performance.

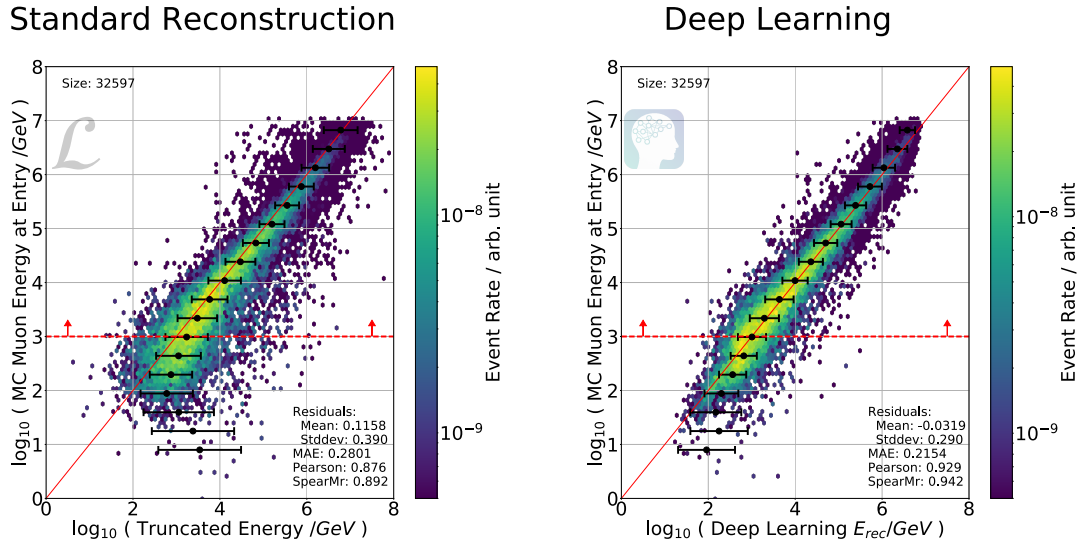


Figure 3: The correlation plots between Monte Carlo truth (y-Axis) and reconstructed energy (x-Axis) are shown for the current standard reconstruction (Truncated Mean [2, p. 18]) and the deep learning approach. The deep learning approach significantly improves the resolution.

One of the target labels reconstructed is the muon energy at its entry into the detector. This is currently the most widespread used proxy for the energy of the primary neutrino. In Fig. 3, the correlation plots are shown for the current standard reconstruction (Truncated Mean [2, p. 18]) and the deep learning approach. It should be noted that the results obtained here are for events of the Online L2 Selection, while additional quality cuts are applied in [2, 10]. The resolution of the reconstruction can be measured in many different ways. For a high resolution, a low standard deviation of the residuals and a high correlation between reconstruction and Monte-Carlo-Truth is expected, as well as a low mean absolute error (MAE). In comparison to the current standard, the deep learning approach can reduce the MAE and the standard deviation of the residuals by over 20%. The standard reconstruction uses the energy loss dE/dx to predict the muon energy. Therefore, it is not well suited for energies below about 1 TeV, where dE/dx is no longer proportional to the muon energy. The deep learning approach does not have this limitation. To obtain a fair comparison, only events with a muon energy above 1 TeV, indicated by the dashed line in Fig. 3, are used to calculate the resolution. The reconstruction of other energy related target labels also yields significant improvements. The directional reconstruction of events, however, currently still remains a challenge. This is further discussed in section 5.

In addition, it should be noted that the deep learning approach is able to reconstruct all events.

The standard reconstructions are only performed if certain quality criteria are fulfilled. The events on which the standard reconstruction is not performed or when it fails are often events which are hard to reconstruct. This could, for instance, be due to events clipping the instrumented volume or to low energetic and dim events. The deep learning approach is still able to reconstruct these events with a resolution comparable to the resolution of the events successfully reconstructed by the standard method.

4. Uncertainty Estimation

In order to get an estimate of the uncertainty on the reconstruction, the network architecture described in section 2 is extended by a small neural network of three fully connected layers. The first fully connected layer of the original architecture is used as input for this new, smaller network. Additionally, a gradient stop is applied to the input, so that the training of the new, smaller network will not affect the original network. The last layer of the new, smaller network has one output node for every target label. It predicts the absolute deviation between the reconstructed and the true value.

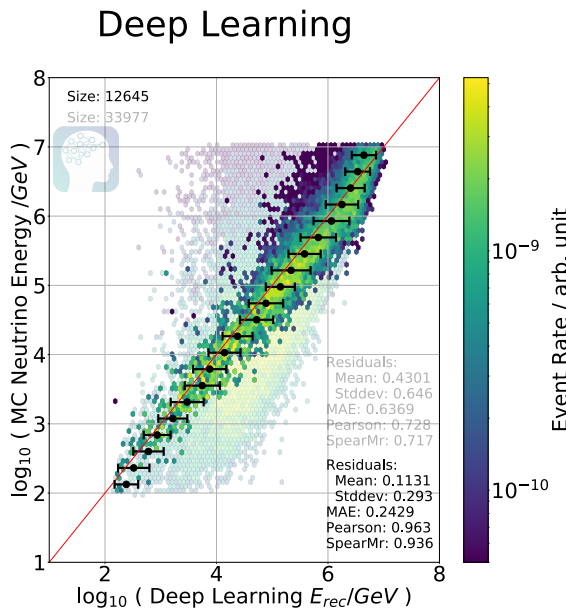


Figure 4: Only the top 10% of events are chosen, in which the neural network estimated the smallest uncertainty. The original sample is shown in the background. In the top left corner, the number of unweighted events is shown for each sample. The uncertainty estimation performed by the neural network can be used to choose a subsample of well reconstructed events, improving the resolution of the neutrino energy by more than 50%, while keeping a tenth of all events.

Although this is just a first guess of the uncertainty, the results are very promising. This can be demonstrated by using the uncertainty estimation performed by the network to select a subsample of well reconstructed events. An example is shown in Fig. 4. It should be emphasized that the reconstruction of the primary neutrino energy is an inherently difficult task.

Moreover, the estimated uncertainty for the deep learning reconstruction can also be used for the standard reconstruction as shown in Fig. 5. Events reconstructed well by the deep learning approach are also well reconstructed by the standard reconstruction. A direct estimation of the uncertainty specifically for the standard reconstruction can be performed to further improve the results. This is of special interest for the standard track reconstruction performed on-site in regard to real time alerts and follow-up observations.

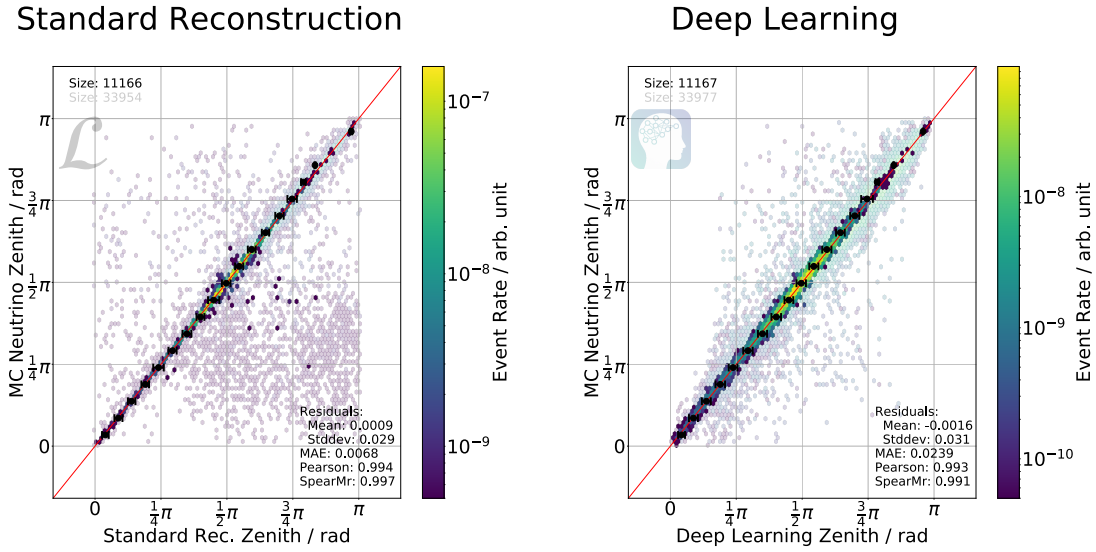


Figure 5: The uncertainty estimation of the neural network for its prediction on the neutrino zenith angle is used to select a sample of well reconstructed events. Although the uncertainty estimation is performed for the deep learning reconstruction, it is also applicable to the standard reconstruction.

5. Directional Reconstruction

The directional reconstruction of events is difficult for various reasons. In contrast to the reconstruction of energy related labels, the directional reconstruction heavily depends on the timing information in addition to the spatial dimensions. Moreover, target labels like the azimuth angle are cyclic. This is difficult in practice with regard to gradient descent minimization. One way of circumventing this is by reconstructing the coordinates of a direction vector separately.

In IceCube, the first pulse registered by a DOM is the most useful for a directional reconstruction, since the photons will have scattered the least. This fact is also used by the standard directional reconstruction currently used on-site which only uses the first pulse as well as the total number of pulses [11, pp. 35 ff]. Therefore, a deep learning approach using these values as input essentially reduces the dimensionality of the problem and should be able to reproduce comparable results. However, while the deep learning approach is able to better reconstruct the direction on average, it currently can not compete with the median and 68%-quantile resolution of the standard reconstruction. Adjusting the loss function from mean squared error to something less outlier sensitive only partially improves the result.

One possible reason for this might be the deviations of the 78 approximately hexagonally arranged strings from an exact hexagonal grid as shown in Fig. 1. The positions of the DOMs deviate up to 35m and about 10m on average off of the perfect virtual hexagonal grid. A convolutional layer assumes symmetry over the input data. However, the deviations break this symmetry which might lead to a worse reconstruction. Investigations are currently underway to validate this assumption. If this holds true, measures can be taken before the convolution in order to correct for these deviations.

6. Conclusions and Outlook

One of the key challenges for an on-site reconstruction is the hardware limitation. The deep learning approach presented here is able to significantly improve the energy reconstruction while reducing the runtime. In addition, the neural network is able to estimate the uncertainty of its prediction as well as the uncertainty of other reconstruction methods. It is therefore well suited for an application at the South Pole. Moreover, the network architecture is not yet fully optimized, but already generates very promising results. Improvements are expected through further optimization.

Currently, a study investigating the effects of an imperfect hexagonal grid is underway. Depending on the results of this study, measures to correct the pulse times for the actual DOM positions can be undertaken. A full integration of the time dimension via a 4D convolution or a combination of a 3D convolution over the spatial dimensions and a recurrent neural network to handle the time dimension might result in an even better performance. Additionally, the third part of the IceCube detector, IceTop, can be integrated as well. Moreover, experience has shown that in most cases training on a specific subset of data with a similar topology converges faster and better than training the same, or a more complex model, on a bigger subset with more event topologies. This leads to the idea of performing an online classification into different topologies. A dedicated network for each topology could then be executed after the classification. This will effectively reduce the complexity of the problem.

7. Acknowledgements

Mirco Hünnefeld acknowledges the support of the Martin-Schmeißer-Stiftung, Germany.

References

- [1] **IceCube** Collaboration, M. Aartsen, et al., *JINST* **12** (2017) P03012.
- [2] **IceCube** Collaboration, M. Aartsen, et al., *JINST* **9** (2014) P03009.
- [3] **IceCube** Collaboration, M. Aartsen, et al., *Astropart. Phys.* **92** (2017) 30 – 41.
- [4] G. Hinton, A. Krizhevsky, et al. in *Advances in Neural Information Processing Systems 25*, pp.~1097–1105. Curran Associates, Inc., 2012.
- [5] Y. LeCun, Y. Bengio, and G. Hinton, *Nature* **521** (2015) 436–444.
- [6] **IceCube** Collaboration, M. Aartsen, et al., *The Astrophysical Journal* **833** (2016) 3.
- [7] M. Abadi, et al. 2016. Software available from [tensorflow.org](https://www.tensorflow.org).
- [8] S. Ioffe and C. Szegedy, *CoRR* [abs/1502.03167](https://arxiv.org/abs/1502.03167) (2015).
- [9] N. Srivastava, et al., *J. Mach. Learn. Res.* **15** (Jan., 2014) 1929–1958.
- [10] **IceCube** Collaboration, R. Abbasi et al., *Nucl. Instrum. Meth.* **A703** (2013) 190–198.
- [11] K. Schatto. PhD thesis, [Mainz U.](https://www.mainz.uni.de), 2014-06-02.

Connecting Beyond the Research Community: IceCube Education, Outreach, and Communication Efforts

The IceCube Collaboration[†], and E. Bechtol[‡], S. Bravo[‡], J. DeMerit[‡], E. Feitlinger[‡]

[†] http://icecube.wisc.edu/collaboration/authors/icrc17_icecube

[‡] Wisconsin IceCube Particle Astrophysics Center (WIPAC), University of Wisconsin–Madison, Madison, WI 53703, USA

E-mail: silvia.bravo@icecube.wisc.edu, james.madsen@uwrf.edu

As an international organization, the IceCube Neutrino Observatory has 48 collaborating institutions, each of which carries out efforts to engage and inform the public. Examples of activities include one-time talks and posts on social media, support for local science and technology programs, and development of visualization tools and inexpensive detectors for student use. In this paper, we describe four successful examples of centrally supported IceCube education, outreach, and communication efforts to reach beyond the research community. First, we give an overview of the field deployments to the South Pole for high school teachers that we have provided in partnership with the PolarTREC program, supported by the US National Science Foundation. This program enables high school teachers to join the IceCube team and experience firsthand the challenges of doing cutting-edge research in the extreme Antarctic environment. Next we describe the IceCube Masterclass, a day-long event held at multiple IceCube Collaboration campuses for motivated high school students. It was offered for the fourth time in spring 2017. After that, we describe science news articles, short summaries of IceCube results and activities, regularly posted on the IceCube webpage and promoted via social media. The last example we discuss are IceCube videos, some produced in conjunction with prominent partners such as TED-Ed, which have been seen by more than two hundred thousand viewers. A few of the most noteworthy IceCube science results have been followed up with in-house-produced videos. For example, a video on IceCube’s sterile neutrino results has received more than ten thousand views. We will provide metrics that describe the reach of these activities along with early efforts to assess the impact of IceCube’s education, outreach, and communication activities.

Corresponding authors: S. Bravo¹ and J. Madsen^{2*}, **Presenter:** E. Feitlinger¹

¹ Wisconsin IceCube Particle Astrophysics Center (WIPAC), University of Wisconsin–Madison, Madison, WI 53703, USA

² Dept. of Physics, University of Wisconsin, River Falls, WI 54022, USA

35th International Cosmic Ray Conference – ICRC217
10-20 July, 2017
Bexco, Busan, Korea

*Speaker.

1. Introduction

The IceCube Neutrino Observatory consists of a cubic-kilometer neutrino detector installed in the ice at the geographic South Pole, between depths of 1450 m and 2450 m, and a square-kilometer surface array known as IceTop [1]. The breadth and depth of the facility's science reach is indicated in Fig. 1 and by the number and variety of contributions submitted for ICRC2017 on behalf of the IceCube Collaboration. Science topics of particular relevance to the ICRC include measuring cosmic ray spectra, composition, and anisotropy; characterizing the astrophysical neutrino flux; searching for neutrino sources; and looking beyond the standard model physics for dark matter, sterile neutrinos, and other exotic particles.

The wide range of IceCube topics, many of which are unfamiliar to all but expert audiences, makes producing effective education, outreach, and communication both challenging and rewarding. Conveying what the IceCube project is doing and why, and telling the stories of the people who make it possible, is a central role of the IceCube project office. In addition, many IceCube Collaboration members also take on this important task, motivated by their enthusiasm for science and to meet funding agency broader impact requirements. Their efforts include giving talks to schools and community groups, hosting local science open houses, participating in associated activities arranged by others, such as the International Cosmic Day [2] or a museum exhibit on detector technology [3], and mentoring high school students. In addition, several IceCube collaborators are working on virtual reality displays of varying degrees of sophistication [4], designing and producing apps that utilize cell phones to capture cosmic ray events [5], and even developing inexpensive stand-alone detectors simple enough for classroom use [6].

This paper will focus on four successful examples of collaboration-wide education, outreach, and communication efforts. The goal is to show how we leverage central resources to reach interested audiences, including those outside the research community. Our efforts involve providing very intensive experiences for a few select K-12 teachers, hosting masterclasses for hundreds of high school students, writing articles on science news updates for our website, regularly reaching thousands, and producing short informational science videos, with 1,000s to 100,000s of views. A brief discussion at the end will describe metrics we are developing to assess the reach and impact of these efforts.

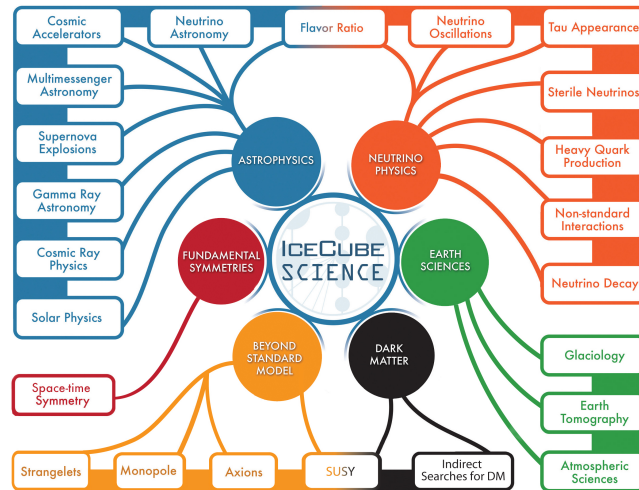


Figure 1: Science topics of the IceCube Neutrino Observatory.

2. Collaboration-wide Examples

The IceCube project maintenance and operations efforts are led by the Wisconsin IceCube Particle Astrophysics Center (WIPAC) at the University of Wisconsin. WIPAC maintains the IceCube website, Facebook and Twitter accounts, and a YouTube channel [7], as digital resources to reach broader audiences. Funding from the maintenance and operation grant is leveraged with other sources and partnerships to support collaboration-wide education, outreach, and communication activities.

2.1 PolarTREC: Field Deployments for Teachers

The NSF-supported PolarTREC program pairs educators, primarily precollege teachers, with polar researchers [8]. The aim of the project is to improve the understanding of the polar regions and the research that takes place there. Teachers are integrated into a research team, participate in a field deployment, and use their skills in translating often arcane, abstract science into accessible language and activities for the classroom. The IceCube project has had five PolarTREC teachers deploy to the South Pole, with the sixth scheduled for the upcoming 2017-18 season¹ (expedition history shown in Fig. 2). We have had success both with teachers we knew prior to selection as well as with those we chose based solely on written application materials and phone interviews.

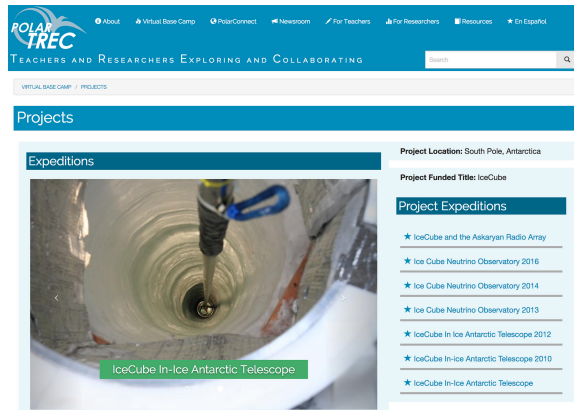


Figure 2: IceCube project history on PolarTREC website [9].

The training of a PolarTREC teacher is a collaborative effort. The IceCube PolarTREC teacher joins a new cohort of about a dozen teachers, who have been assigned to research projects in the Arctic and Antarctic, for a week in Alaska in February. They learn about expectations for the PolarTREC program and resources available for support, and they network with past PolarTREC teachers. The IceCube teachers generally deploy to the South Pole for about three weeks in late December or January. This leaves a little less than one year for the teacher to be integrated into the IceCube project. They learn about IceCube science, receive specific training for tasks they will carry out while deployed, and plan education and outreach

activities to maximize the impact of their experience.

Working with the PolarTREC program enriches IceCube, the teacher, and their communities. The teachers are highly motivated, excited, and anxious to convey what they are learning. They bring their unique perspectives and skills, and they develop materials that document their experiences, including videos, journals, and photos that are posted in real time and then archived on their PolarTREC web page. In addition, their deployments provide a pulse of activity that captivates

¹ AMANDA, the proof-in-concept project prior to IceCube, hosted three additional teachers [10].

local and national media and brings awareness of IceCube research to new and diverse audiences. For example, Puerto Rican educator Armando Caussade's deployment received extensive coverage throughout Puerto Rico, including print and broadcast media. He posted all of his materials on his PolarTREC web page [11], in both Spanish and English, and published a book based on his trip, "A Puerto Rican in the South Pole" [12]. Other video resources produced by IceCube PolarTREC teachers are described in Sec 2.4.

2.2 IceCube Masterclass: Intensive Day-long Experiences for Students

In 2014, IceCube launched the IceCube Masterclass [13], an educational research-based program for high school students that aims to excite the next-generation of researchers in astrophysics. The IceCube Masterclass program was inspired by the International Masterclasses program, started in 2005 by the International Particle Physics Outreach Group, and supported in the U.S. by QuarkNet [14].

During a masterclass, high school students, and sometimes accompanying teachers, join an IceCube institute for a day to engage in real research and experience an authentic and international scientific environment. Students are guided through one IceCube analysis, either the discovery of astrophysical neutrinos or the measurement of the cosmic ray spectrum [15]. The focus is to illustrate how astrophysics is done by reproducing an important IceCube paper, condensing the steps to allow the exercise to be completed in a few hours and avoiding the technicalities of handling large amounts of data.

The first IceCube Masterclass hosted around 100 students at five institutions in the U.S. and Europe. The fourth edition took place in March 2017 with over 200 students in Belgium, Denmark, Germany, and the US, at a total of 14 institutions. The activities were designed for students in their last two years before college, although a few younger students who were especially interested in astrophysics have also participated.

Each year, the program is evaluated using pre- and post-program surveys containing a mix of open-ended, multiple-choice, and rating questions [16]. Students showed gains in knowledge and skills, and they left feeling more excited about science and physics. They were asked to assess each activity of the day on a scale of 1–5. The analysis activity ranked highest, with an average score per institution above 4.

2.3 Detector and Research News: a Feed for the IceCube Website and Social Networks

The IceCube website publishes on average two news articles every week. These include weekly updates about activities at the South Pole, summaries of every research paper published by the IceCube Collaboration, features on detector operations or outreach activities, and press releases and announcements about outstanding results and awards honoring the IceCube Neutrino Observatory and/or the international team behind it. These news items are the main dynamic content of the website and also feed IceCube Facebook and Twitter accounts.

These news posts consistently account for around 10% of the page views on the IceCube website, but their impact is much larger in terms of audience reach and overall IceCube awareness. Although only 50% of these articles get over 1,000 readers on the website, and less than 20% reach 3,000 readers or more, they trigger a shower of communication that can amplify our audience by a factor of 10 or more.

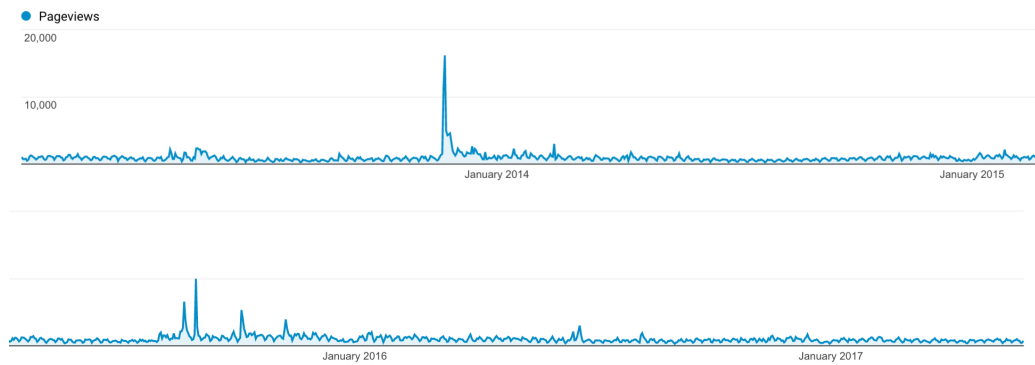


Figure 3: Daily page views of IceCube’s website since 2013. The largest peak corresponds to the publication in *Science* of the discovery of astrophysical neutrinos.

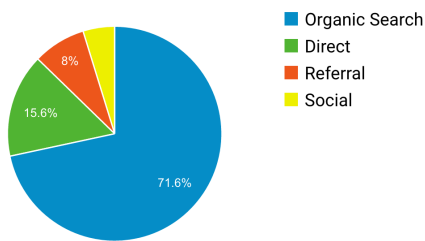


Figure 4: Top channels bringing traffic to IceCube’s website.

On an average day, over 400 users visit the IceCube website, and 25% of those are returning visitors. This number varies considerably, with peaks that correspond to the publication of articles (see Fig. 3). The most successful news article—the press release about the discovery of astrophysical neutrinos published in *Science* in November 2013 [17]—brought in over 10,000 users in less than 48 hours. However, a closer look at the data shows that although this peak was triggered by the release, not all users came to our website to learn about the discovery. Only about half (4,702) of the 10,000 users read that news during those two days (currently the news has over 7,400 views). So, thousands of visits were triggered by the news in the media, or on social networks, and came to the website to learn more about IceCube. This effect is confirmed by comparing the page views of the first five months of 2017 with five months around the *Science* paper. The percentage of views of IceCube news was in both cases around 11%, i.e. the effect of the discovery was diluted when taking into account the views over a few months. However, the visits to the home page increased by 30%, with a huge peak around the IceCube discovery (visits to the home page usually are in the few hundreds per day, and were over 5,000 the day of the release). At the same time, the percentage of visits to static sections, such as science, outreach or the collaboration, decreased by 50% or more. The readers of content related to the South Pole remained stable at around 15%, showing the appeal of Antarctica for all audiences.

The increase in visits to the home page can be easily explained if we look at the origin of website users, who mostly reach IceCube content as a result of an organic search, i.e., after looking for content by entering key words in a browser search engine (see Fig. 4 for distribution).

A similar cascade effect is observed on IceCube social networks. On Facebook, with just over 8,000 followers, posts of research news that have one or two thousand readers, can easily reach 5,000 to 10,000 followers, and only a few of them (typically around a 5%) will actually click on the news link. This amplifying effect can also be observed in the patterns of new likes on Twitter

that mimic the impact of IceCube news on this social network. IceCube's Twitter feed currently has around 6,200 followers. Fig. 5 shows recent Twitter activity.

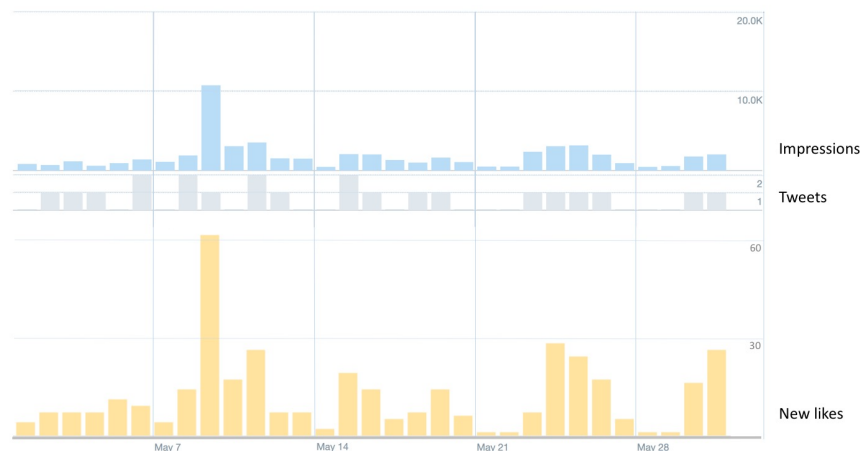


Figure 5: Twitter impressions in May 2017 (blue) and number of tweets (grey). The yellow graph shows the number of new likes for the same period.

2.4 IceCube Videos: In-house and Partner Productions

In the era of mobile devices and multimedia content, it is well known that animated graphics and video productions can engage much larger audiences than text-based content and static images. However, production of multimedia resources takes more human and capital resources. IceCube uses a strategy that leverages internal resources by combining in-house and partner productions. We have worked with the TED-Ed portal (Fig. 6), Spanish filmmaker Javier Diez, the Milwaukee Public Museum, and the American Physical Society to produce several videos introducing IceCube to the public. As of May 2017, they have reached over 210,000 views [18, 19, 20, 21].

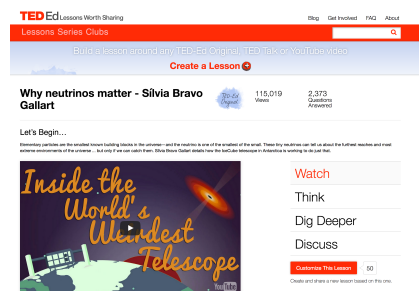


Figure 6: TED-Ed lesson about IceCube, including a video and questions for using the lesson in formal and informal learning.

Several of the PolarTREC teachers have also produced videos prior to and during their visits to the IceCube Neutrino Observatory at the South Pole. During her deployment in January 2017, teacher Kate Miller published a video touring the South Pole station that currently has almost 175,000 views. In 2009, another PolarTREC teacher, Casey O'Hara, produced a novel stop-motion animation about IceCube that continues to be popular, and has around 23,500 views [22, 23].

During the last year, IceCube has also internally launched the regular production of short videos, including a series featuring IceCube research. The first of these videos, in conjunction with a press release about a search for sterile neutrinos, has accumulated over 14,000 views on the IceCube YouTube channel, and several thousand more viewers on the websites of Wall Street Journal and Space.com [24].

3. Education, Outreach and Communication Metrics

We are currently working on a new and broader evaluation framework to assess the impact of IceCube activities, with a special focus on measuring the accomplishment of main goals related to target audiences. The aim is to move beyond only measuring and reporting the number of web users, Facebook and Twitter followers, video viewers, or participants at outreach programs and events. This framework is mostly implemented in the evaluation of the IceCube Masterclass outreach program, with the long-term goal of measuring the impact this intensive activity (about eight hours of contact per participant) has on fostering research careers.

For other IceCube activities, we are just starting to move beyond recording the number of our participants and gather demographic information on our audiences. A common goal of IceCube communications and outreach programs is to reach and serve target communities, such as groups underrepresented in science careers, K-12 students and teachers, science aficionados, and the broader IceCube community. Online platforms such as websites and social networks have analytic tools to parse simple metrics, for example, gender and home country or language.

Preliminary studies about gender reach show a predominantly male audience, with only 22% of IceCube followers being women on Twitter, 27% on Facebook, and 32% on the IceCube website. Gender metrics are from Google Analytics summaries.

Regarding origin, IceCube’s audience is primarily from English-speaking locations. English is the language used on all IceCube official communication channels, and English-speaking countries, including the US, Canada, Australia, and the UK, host more than 50% of the IceCube institutions. However, small efforts towards multilingualism are already showing that this audience can be diversified. The minisite of the IceCube Masterclass published the same content in three languages: English, German, and Spanish. On this website, Germany is second in the number of users—it is the fourth on the main website. The list of the top 10 countries in the masterclass website also includes Spain and Mexico, countries that do not show up in the top 10 countries for the main website (see Table 1 for reference).

On a wider scope, IceCube has not yet implemented a collaboration-wide assessment model. This would allow the aggregation of data from the vast number of programs and activities run by the education and outreach office at UW–Madison, headquarters of the IceCube Neutrino Observatory, together with local programs at each IceCube institution (48 in 12 countries). A design for such a model is currently under development. It will include the identification of the relevant metrics based on recent research on the assessment of broader impacts and the creation of a flexible tool that can be used by IceCube collaborators around the world.

4. Summary and Outlook

The impact of science extends beyond the knowledge and technology produced. Increasingly, research funders are requiring scientists to engage in education, outreach, and more formal efforts

IceCube	
Main website	Masterclass minisite
US	US
UK	Germany
India	UK
Germany	Russia
Canada	Spain
Australia	India
Russia	Belgium
Italy	Italy
Japan	Mexico
France	Japan

Table 1: List of the top 10 countries for the main website and the masterclass minisite.

to communicate beyond the traditional research community. The expectations and investments in these activities scale with the size of the project. Four examples of IceCube's ongoing, centrally supported education, outreach, and communication efforts were described. These activities are providing ways to connect to IceCube science and personnel on a variety of levels and formats. They range from research experiences including field deployments for teachers and masterclasses for high school students that provide intensive, face-to-face contacts to digital resources like weekly web news and video content. We have good data on the number of people who consume media or participate in events. The next step is to learn more about who these people are to ensure that the desired audiences are being reached, and that activities are having the desired impact.

References

- [1] **IceCube** Collaboration, M. G. Aartsen et al., *JINST* **12** (2017) P03012
- [2] International Cosmic Day: <https://icd.desy.de>
- [3] IceCube exhibit at Gustavianum Museum in Uppsala: <http://www.gustavianum.uu.se/gustavianum-eng/exhibitions/temporary-exhibitions/aspiring-to-precision/the-exhibition/iceCube>
- [4] Polar Virtual Reality project at Wisconsin Institutes of Discovery: <https://pvre.discovery.wisc.edu>
- [5] DECO: <https://wipac.wisc.edu/deco/home>
- [6] S. Axani, J. Conrad and C. Kirby, arXiv:1606.01196 [physics.ed-ph]
- [7] <http://icecube.wisc.edu>; https://twitter.com/uw_icecube; <https://twitter.com/UWastrophysics>; <https://www.youtube.com/channel/UCqhYPTo6SWmi5bbVBmUf9NA>
- [8] PolarTREC: www.polartrec.com
- [9] IceCube PolarTREC expeditions: <https://www.polartrec.com/projects/icecube-project>
- [10] See Muhs, Pettersson, Petula, http://tea.armadaproject.org/tea_meetteachers.html#antarctic
- [11] Armando Caussade's PolarTREC page: <https://www.polartrec.com/member/armando-caussade>
- [12] "A Puerto Rican in the South Pole": <https://www.polartrec.com/resources/article/a-puerto-rican-in-the-south-pole>
- [13] IceCube masterclass: <https://masterclass.icecube.wisc.edu>
- [14] International Particle Physics masterclass: <http://www.physicsmasterclasses.org>
- [15] **IceCube** Collaboration, *POS(ICRC2015)* 576 (2016).
- [16] "Searching for Cosmic Neutrinos in IceCube, an IceCube Masterclass research-based activity," *Physics Teacher*, in press.
- [17] **IceCube** Collaboration, M. G. Aartsen et al., *Science* **342** (2013) 1242856
- [18] "Why Neutrinos Matter," <http://ed.ted.com/lessons/why-neutrinos-matter-silvia-bravo-gallart>
- [19] "Neutrino, Measuring the Unexpected," <https://vimeo.com/114361247>
- [20] "Chasing the Ghost Particle," <https://wipac.wisc.edu/ghostparticle>
- [21] "IceCube Explained," https://www.youtube.com/watch?v=xUit5_B9k-U
- [22] "Tour of South Pole Station," <https://www.youtube.com/watch?v=vrPiVT23MhA>
- [23] "IceCube - Animated Overview," <https://www.youtube.com/watch?v=aMnGWqoDaAA>
- [24] "The Search for Sterile Neutrinos in IceCube," <https://www.youtube.com/watch?v=tIMoFsRlrew>